3. Mechanical testing of biological materials

In this chapter, the methods for *in situ* mechanical testing described in Chapter 2 are applied to a variety of biological materials. Their observed mechanical performance and property values are discussed with reference to those found by other techniques in the literature.

3. 1 Introduction

Using conventional testing methods, it is not possible to resolve the mechanical properties of biological materials at a level of their hierarchy, which is currently of particular interest: that at the micrometer scale. At this level, the structures of interest, such as a single seta of the hairy attachment system of a beetle or a sensory organ of an insect, are difficult to handle already during sample preparation, due to their complex geometry and their small size. This size also imposes stringent requirements on strain and force resolution and creates the need for *in situ* microscopic observation, which existing devices (described in the literature review of Chapter 2.1) do not possess. How the micromanipulator-based testing device presented in this thesis overcomes these problems and makes measurements possible of Young's modulus, tensile strength and strain to failure, is illustrated below. Its versatility makes it equally well suited to perform beam bending and tensile tests as well as tests in compression. The preferred mode of testing can be chosen according to the sample material and geometry. Examples are described for testing in bending and in tension using materials and structures which are currently receiving great research interest. These are horse hair and spruce wood cell wall material tested in bending, and insect cuticle as well as natural and biomimetic silk fibres tested in tension.

3.2 Beam bending

Beam bending experiments on cantilever shaped samples were carried out in an SEM (Leo 1530 VP) after sample preparation in the FIB (see Chapter 2.3.1 for details). Samples were coated with a thin carbon layer in order to minimise charging effects during sample preparation and mechanical testing. Great care was taken to ensure that the stiffness of the AFM tip was at least one, better two, magnitudes higher than the stiffness of the samples so that the deflection of the AFM tip during loading could be neglected. The stiffness of the cantilevers was estimated before each test; the results are listed below.

3.2.1 Calibration demonstrated on Kapton®

Initially, beam bending experiments were carried out on Kapton® as a reference material for which the material properties are well known. For sample preparation, a small piece of Kapton® foil was clamped into a custom made cubic sample holder. This sample holder has two stubs on neighbouring sides so that the sample can be tilted by 90°. This eases the preparation of samples with a rectangular cross-section. It also means that the sample orientation can be rotated after the micromachining process so that a side view of the sample during the bending test is possible without having to remove it from the sample holder.

The Kapton® cantilever (Figure 3.1) was micromachined to be 248.3 µm long, 15.4 µm wide and 13.1 µm thick. Figure 3.2 shows the cantilever and the micromanipulator ready for testing. Measurements were taken at eight different positions along the length of the sample. For testing, the micromanipulator was moved stepwise towards the sample and a micrograph was taken for each step, as described in Chapter 2.4.

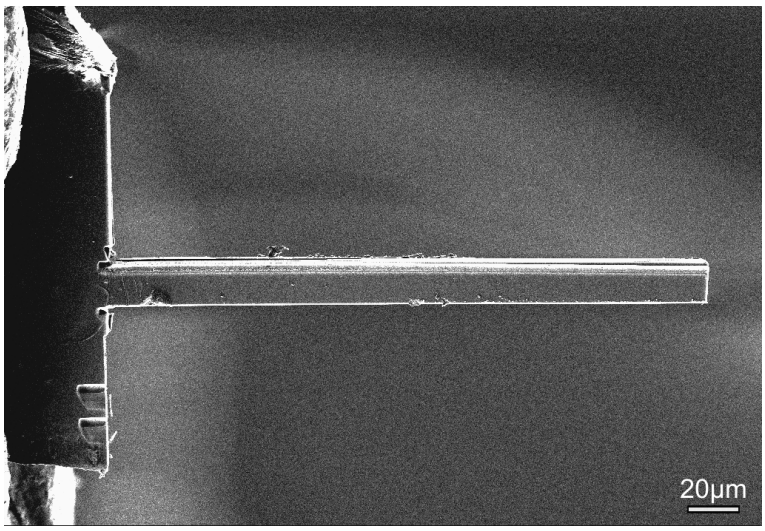

Figure 3.1: Kapton® cantilever (SEM micrograph, FIB milling parameters: beam current = 1000 pA for milling, 70 pA for cleaning, dwell time = 1.0 µs, overlap = 50%).

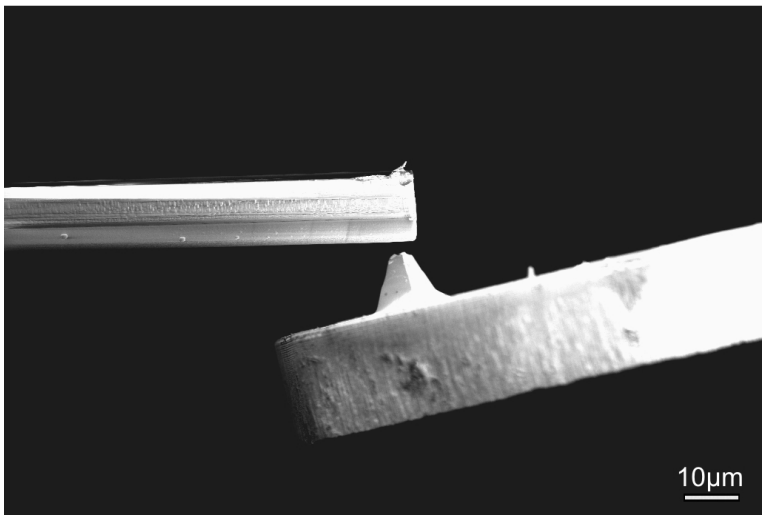

Figure 3.2: AFM tip close to the Kapton® cantilever, ready for testing (SEM micrograph).

For each position along the sample, the beam length, the force and the displacement during loading and unloading were determined. After the tests, the force was plotted versus the displacement for each run. Figure 3.3 shows one of the force versus displacement plots. The sample shows an elastic behaviour during both its loading and unloading. The hysteresis in the measurements is due to a hysteresis of the piezo used for the AFM tip.

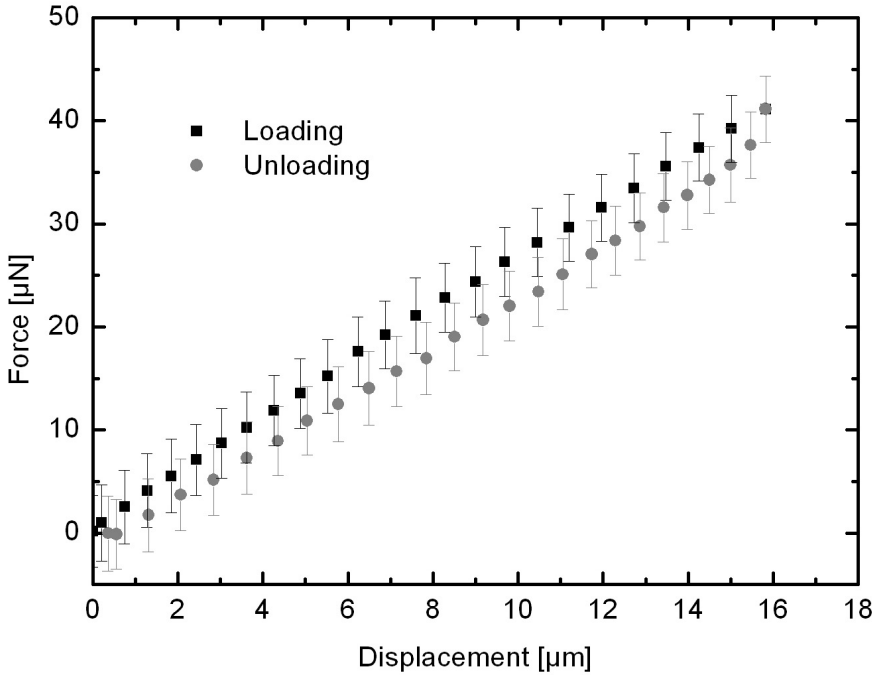

Figure 3.3: Force versus displacement of a single test on a Kapton® cantilever (error-bars of the displacement fall within the size of the symbols).

After plotting the loading and unloading curves, a straight line was fitted to each. From the slope of the line and the length, width and height of the cantilever, the Young's modulus was calculated according to Equation [2.4] (error calculation in Appendix 6.3). Table 3.1 lists the

Young's modulus for each of the positions along the cantilever and for both loading and unloading. The mean value of the Young's modulus calculated from the loading curve is 3.73±0.60 GPa, from the unloading curve 3.60±0.54 GPa. Force versus displacement plots for all tests on Kapton® are given in the Appendix 6.2.

Table 3.1: Young's modulus calculated from the loading and unloading curves measured at different positions along the length of the cantilever.

Cantilever length [µm]	Estimated cantilever stiffness [N/m]	Young's modulus loading [GPa]	Young's modulus unloading [GPa]
240.04	2.26	3.54±0.69	3.62±0.51
238.15	2.31	3.76±0.59	3.61±0.50
236.89	2.26	3.77±0.65	3.47±0.56
235.03	2.45	3.82±0.68	3.67±0.59
233.18	2.51	3.77±0.63	3.68±0.58
227.92	2.62	3.67±0.60	3.58±0.59
223.07	2.81	3.69±0.59	3.60±0.52
215.63	3.06	3.85±0.38	3.54±0.50

The Young's moduli obtained from the beam bending experiments were compared with those obtained by nanoindentation on 125µm thick Kapton® foils from the same manufacturer. The mean value of the Young's modulus obtained from 40 indents at an indentation depth of 500 nm was 3.48±0.08 GPa. In the technical data sheets of Goodfellow, the distributor of the Kapton® foils, a Young's modulus of 2.0 to 3.0 GPa (measured in tension, Goodfellow) is given. The results of the Young's moduli agree, considering the different testing methods, which deliver different moduli. This proves that the newly developed *in situ* testing method produces reliable results.

3.2.2 Test on a hair from a horse tail

To illustrate that the method is also well suited for the testing of biological fibres, the Young's modulus of a hair from a horse tail was measured. As human fingernails and hair, feathers and hoofs, horse hair consists of keratin. For the test, a single hair with a diameter of 156 µm was cut to a length of 3167 µm, clamped into a specimen holder and approached by the AFM tip (Figure 3.4).

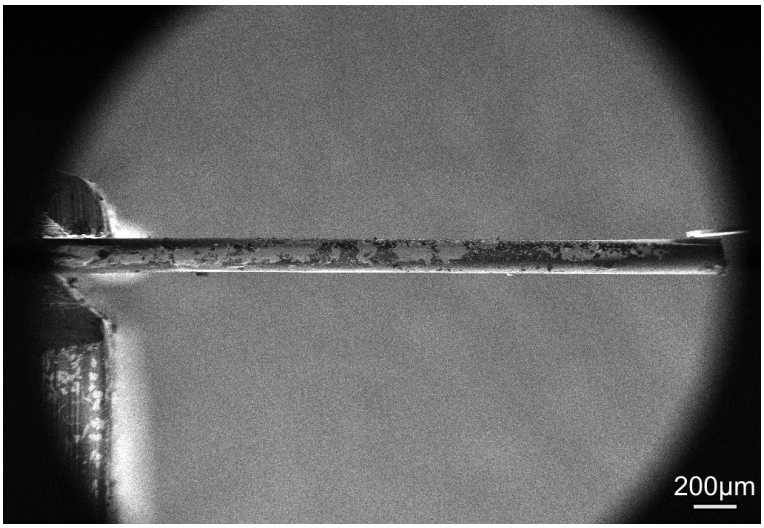

Figure 3.4: Horse hair clamped in a specimen holder. The AFM tip of the micromanipulator is in contact at the end of the specimen (SEM micrograph).

As before, bending tests were performed at different positions along the length of the sample, and the load versus the displacement was recorded (Figure 3.5).

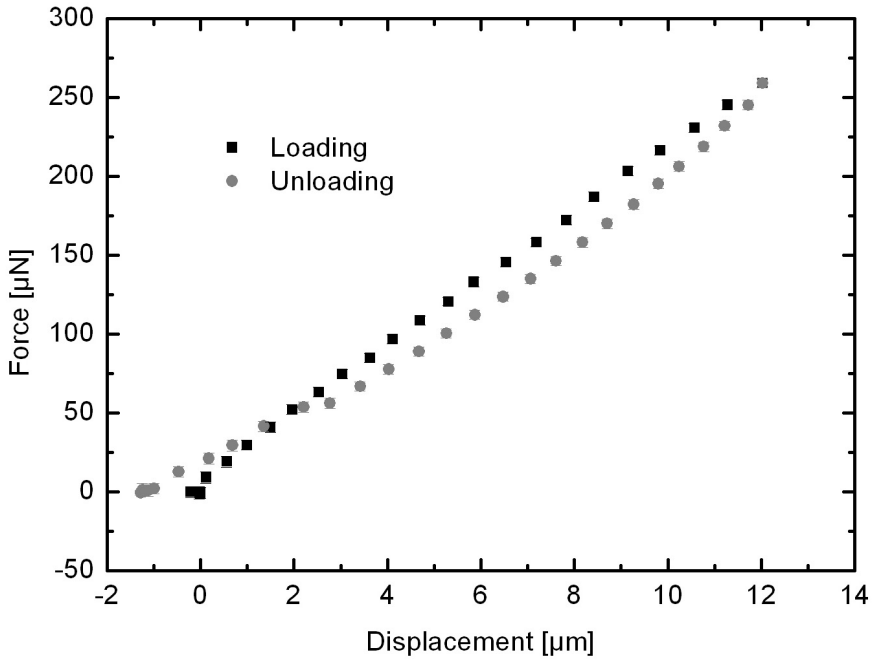

Figure 3.5: Force deflection curve of a single test on horse hair (error-bars fall within the size of the symbols).

Table 3.2 lists the Young's modulus for each of the positions along the cantilever and for both loading and unloading. The Young's modulus (calculated using Equation [2.5], error calculation in Appendix 6.3) from the loading curve is 6.28±0.66 GPa, the mean value of the Young's modulus calculated from the unloading curve is 6.37±0.64 GPa. The force versus displacement plots of all runs are listed in Appendix 6.2.

Table 3.2: Young's modulus of a horse hair (keratin), calculated from the loading and unloading curves measured at different positions along the length of the cantilever.

Cantilever length [μm]	Estimated sample stiffness [N/m]	Young's modulus loading [GPa]	Young's modulus unloading [GPa]
3116.0	16.11	5.59±0.72	6.33±0.68
3087.0	17.54	5.91±0.69	6.93±0.67
3054.0	19.47	6.36±0.65	6.32±0.72
3048.7	21.21	6.89±0.58	6.57±0.56
3049.3	20.38	6.62±0.70	5.70±0.60

3.2.3 Properties of spruce (*Picea sp.*) wood cell wall

Mechanical testing in tension or bending of spruce (*Picea sp*.) wood cell wall material was to date restricted to mechanically or chemically obtained whole cells. A more site-specific sample preparation and testing was not available. With the method presented here, it was possible to prepare, with high precision, cantilevers from an individual wood cell, called tracheid. Tracheids are long hollow cells, composed of up to 50 % largely crystalline cellulose fibrils wound in a spiral fashion around the longitudinal cell axis. The cellulose fibrils are embedded in a matrix which consists of equal parts of hemicellulose (a polysaccharide mixture) and lignin (a phenolic polymer) (Dinwoody, 2000). Tracheids have a length varying from 2 to 4 mm, a diameter of 20 to 40 μm and a wall thickness of 2 to 10 μm. The tracheid wall can be divided into four different layers: the primary wall and the three secondary cell wall layers S1, S2 and S3. The S2 layer is the thickest and mechanically most important and forms up to 80% of the entire cell wall thickness (Dinwoody, 2000).

Tests were performed on a single spruce cell wall. Samples were prepared from a razorblade cut slice of spruce wood (Figure 3.6). The resulting wedge was clamped into a sample holder and mounted in the FIB system to cut a cantilever from cells of medium wall thickness (Figure 3.7).

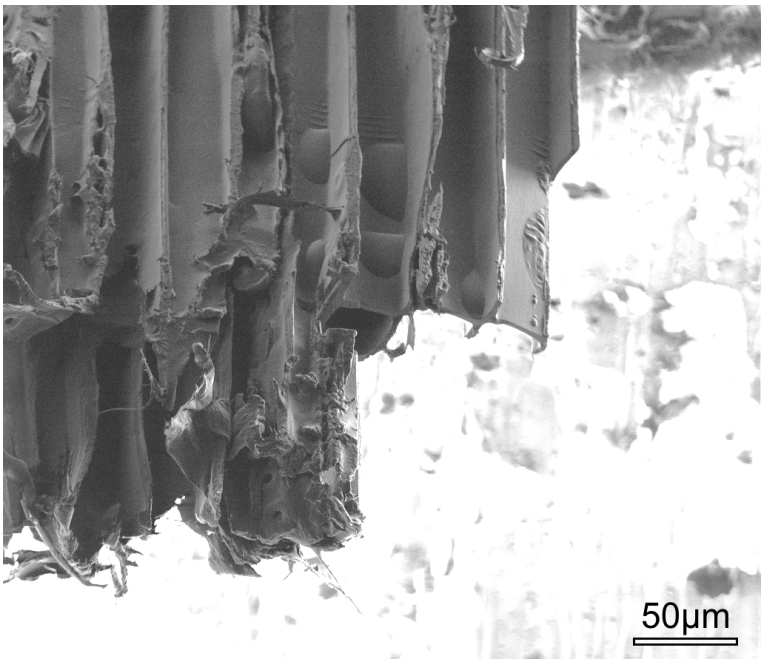

Figure 3.6: Single wood cells (tracheids) of a small piece of spruce wood (FIB micrograph).

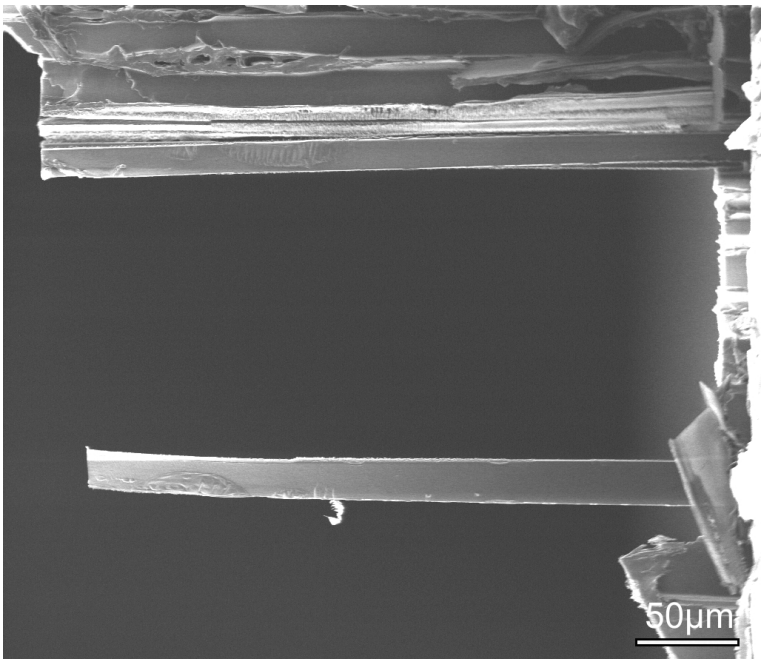

Figure 3.7: Free standing spruce wood cell wall (FIB micrograph, milling parameters:
beam currents = 350 pA for milling, 70 pA for cleaning, dwell time = 1.0 µs, overlap = 50 %).

The cantilever was 353.0 µm long, 17.39 µm wide and 3.47 µm thick. Figure 3.8 shows a cross-section of the cantilever.

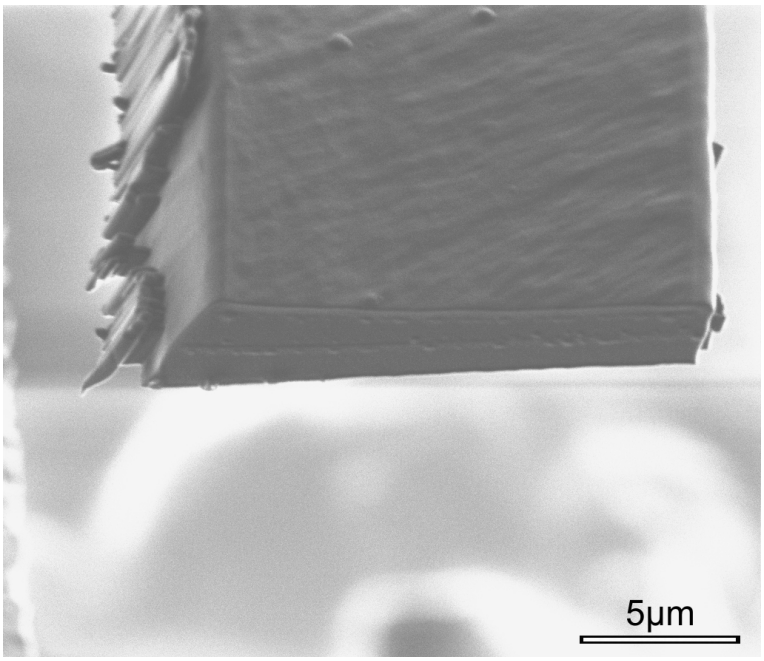

Figure 3.8: Cross-section of the spruce wood cell wall cantilever (FIB micrograph, milling parameters: beam current = 150 pA for milling, 11 pA for cleaning, dwell time = 1.0 µs, overlap = 50 %).

Since the stiffness of the cell wall was low, bending tests for a cantilever longer than 134 µm showed a poor signal to noise ratio in the force measurements. Thus the cantilever was tested for lengths shorter than 134 µm. Figure 3.9 shows the force deflection curve of a test of a single spruce wood cell wall cantilever.

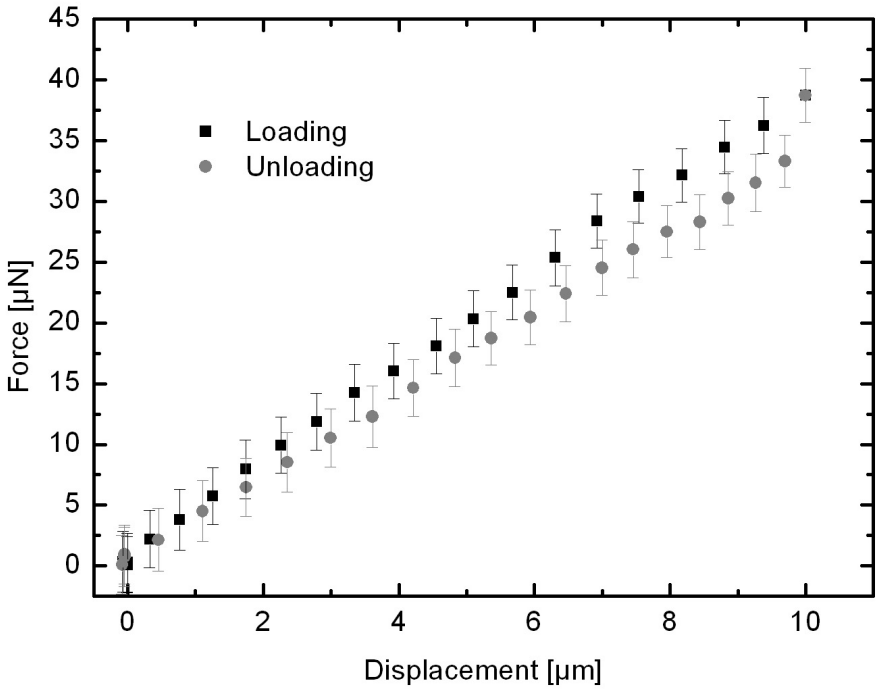

Figure 3.9: Force deflection curves of a spruce wood cell wall cantilever, tested in bending (error-bars of the displacement fall within the size of the symbols).

Again, a straight line was fitted to the loading and unloading curves. From the slope the Young's modulus was calculated using Equation [2.4] (error calculation in Appendix 6.3). The calculated values are listed in Table 3.3:

Table 3.3: Cantilever length, and the Young's modulus calculated from the loading and unloading curve.

Cantilever length [µm]	Estimated sample stiffness [N/m]	Young's modulus loading [GPa]	Young's modulus unloading [GPa]
134.1	1.88	31.3±5.8	28.3±5.9
122.8	2.44	25.6±3.1	24.0±4.0
114.0	3.05	30.5±4.4	26.7±4.0
109.8	3.42	27.1±3.3	24.7±2.7
108.1	3.58	26.2±3.2	24.0±3.4

The mean value of the Young's modulus calculated for the loading curve is 28.2±4.0 GPa, the Young's modulus calculated for the unloading curve is 25.6±4.0 GPa. Force versus displacement plots for all runs are listed in Appendix 6.2.

3.3 Tensile testing

Tensile tests were performed *in situ* in a FIB (fei 200 xP) system. Particularly for materials with a composite structure or a complex geometry it is the preferred method to determine mechanical properties. The FIB provides the advantage that sample preparation, testing and analysis can all be performed consecutively *in situ*. In contrast to the bending test, the samples could be tested in their natural state without carbon coating.

3.3.1 A single seta of the beetle *Gastrophysa viridula*

The mechanical properties of individual setae of hairy attachment systems found in insects and geckos, such as those of the beetle *Gastrophysa viridula* (Figures 1.3 and 1.4), have recently received a great deal of research attention (Gorb, 2000). Their adhesive pads are unique in that they are covered by finely structured contact elements. These hairs, or setae, form a brush-like structure and end in contact elements having an area of only a few square micrometers. In insects, the pads themselves consist of a chitin-fibre composite known as insect cuticle, and in geckos they consist of keratin. In insects, the setae on these pads are several tens to a hundred micrometers in length and a few micrometers in diameter, whereas in geckos they have a hierarchical structure ending in contact elements in the sub-micrometer

range. In each species, the setae terminate in spatulae, which adhere to almost any surface by van der Waals forces (Autumn *et al.,* 2000; Autumn *et al.,* 2002). Models have been developed to describe the adhesion of such attachment devices, based on the Johnson-Kendall-Roberts (JKR) theory of contact mechanics (Arzt *et al.,* 2003; Spolenak *et al.,* 2005).

The Young's modulus, tensile strength and radius of the seta were found to be critical parameters for the performance of the attachment devices. Most recently, adhesion design maps have been developed that delineate the material properties and dimensions required for optimal adhesion (Spolenak *et al.,* 2005). However, the mechanical properties of single setae have, to date, not been determined. In the following, the first measurements of Young's modulus, tensile strength and strain to failure of an individual seta of the beetle *Gastrophysa viridula* (Figure 3.10) are described.

Figure 3.10: Beetle *Gastrophysa viridula* (Digital camera).

For mechanical testing of individual setae, the terminal five segments of a beetle's leg were mounted with silver paint onto a small metal block on the sample holder and placed in a FIB (fei 200 xP) without further sample preparation. The AFM tip was brought into contact with the free end of a seta and affixed to it by sputtering onto its end a tungsten tape of 1 µm thickness. The seta was then cut at its base with the FIB and transferred to a block of metal onto which it was mounted with a second tungsten tape. After sample preparation, the tensile

test was performed as described above in Chapter 2.3.2. Figure 3.11 a) shows the seta ready for testing: the attachment pad on the AFM tip and the opposite end on the supporting metal block. Figure 3.11 b) shows the ruptured seta after the test.

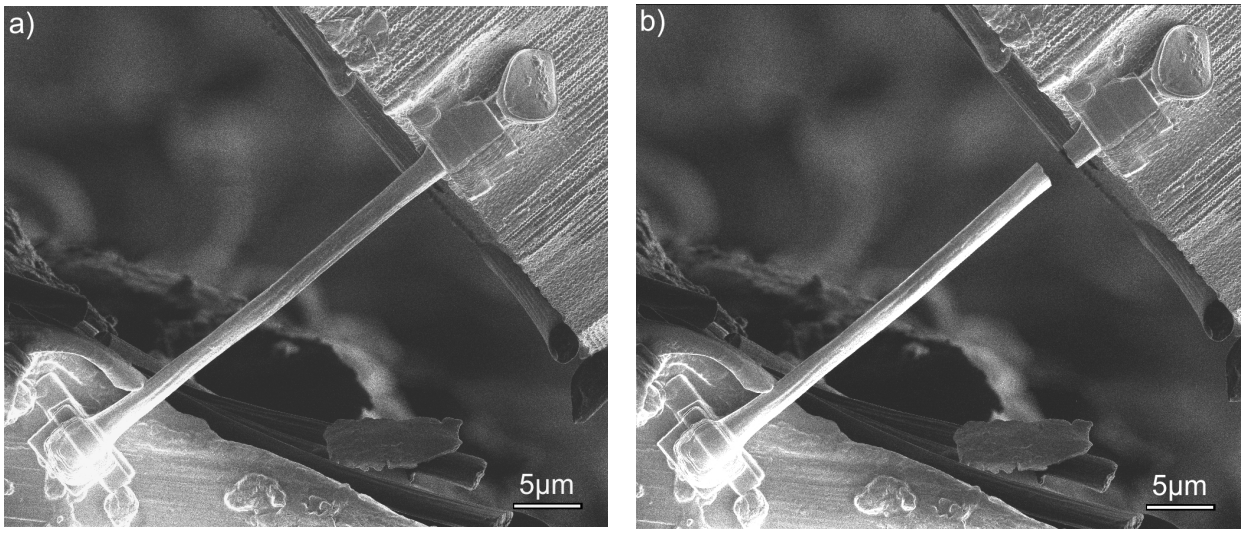

Figure 3.11: a) Single seta of the beetle *Gastrophysa viridula* glued between the AFM tip in the upper right and with the opposite end on the supporting metal block. b) Ruptured seta after the tensile test (FIB micrographs).

After the tensile test, the FIB system was used to prepare several cross-sections along the length of the seta (Figure 3.12). The cross-sections revealed that the seta has a hollow core, the mean porosity of the seta was calculated to be 0.14 %. From the cross-sections the mean cross-sectional area was calculated to be 1.94±0.33 µm^2, subtracting the area of the pores.

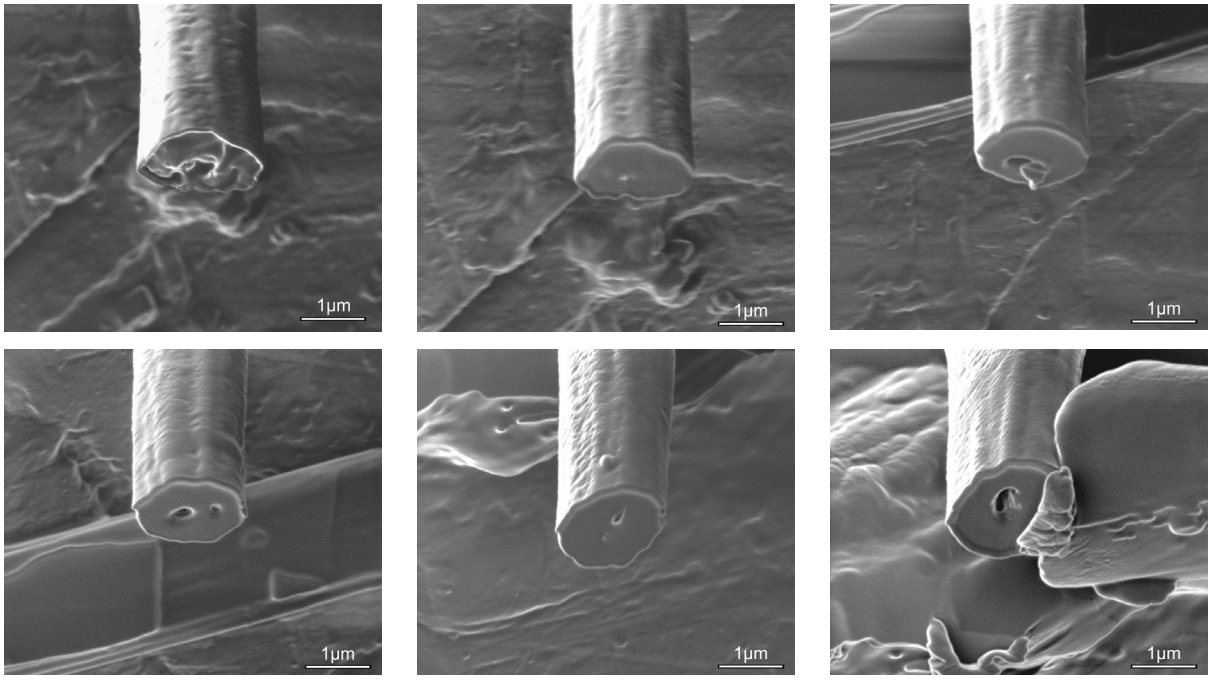

Figure 3.12: Fracture surface after the test and cross-sections cut with the FIB. The mean cross-sectional area is 1.94±0.33 µm^2 (FIB micrographs, milling parameters: beam current = 150 pA for milling, 11 pA for cleaning, dwell time = 1.0 µs, overlap = 50 %).

Another interesting observation was that the seta does not seem to consist of a uniform material, but rather of two, an outer shell (light in colour) around a hollow core (darker than the shell), which probably have dissimilar materials properties. Further investigations are required to confirm this hypothesis.

Image analysis software was use to determine strains from the micrographs (Chapter 2.6). The stress was calculated from the measured force, divided by the mean cross-sectional area, excluding the area of the hollow core. Figure 3.13 shows the first tensile stress-strain plot for a single seta of the beetle *Gastrophysa viridula* (error calculation in Appendix 6.3). Table 3.4 lists its mechanical properties.

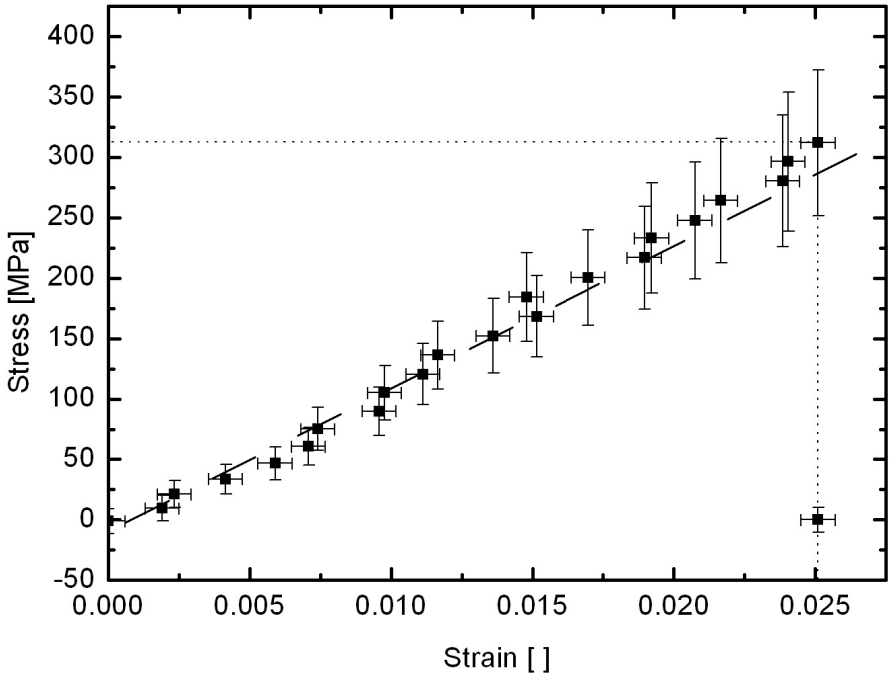

Figure 3.13: Stress strain curve of a single seta of the beetle *Gastrophysa viridula*.

Table 3.4: Material properties of a single seta of the beetle *Gastrophysa viridula*.

Sample	Young's modulus [GPa]	Tensile strength [MPa]	Strain to failure [%]	Strain rate [nm/s]
Beetle seta	11.2±1.0	309±60	2.51±0.06	2.0

3.3.2 Natural (*Araneus diadematus*) and artificial spider silk

For a number of years, researchers have tried to emulate natural spider silk properties in man-made fibres, with limited success. Here we compare the properties of dragline threads of the garden cross spider (*Araneus diadematus*) with that of artificial silk fibres produced in the laboratory of Dr. Thomas Scheibel, TU Munich.

Natural spider silk versus artificial spider silk

Spider silks are attractive biological materials due to their exceptional mechanical properties: a combination of a high tensile strength with a high strain to failure and a resulting remarkable capacity to absorb energy. So far their efficiency (performance per weight) is unrivalled by man-made materials. Because of their excellent mechanical properties and other attractive characteristics such as good biocompatibility and biodegradability, spider silk has a lot of potential for numerous technical and medical applications. The fabrication of very strong, but light ropes, bullet proof clothing, and the use of spiders silk for the stitching of wounds, are examples. Lacking so far are processes with which artificial spider silk can be synthesised in large quantities and with the same properties of natural spider silk. Thus the development of routes for large scale production of artificial spider silk with the characteristics of natural ones and of reproducible and constant quality is the goal of various industrial and scientific research groups (Lazaris *et al*., 2002; Menassa *et al*., 2004; Huemmerich *et al*., 2004).

There are several different kinds of spider silk. Here, we concentrate on the dragline silk of orb-web weaving spiders. It is used for the production of the mooring threads, framework threads and radials in the web, and for the spider's lifeline (Pérez-Rigueiro *et al.,* 2001; Dai *et al.,* 2003). Of the different kinds of silk which a spider produces, the drag line has the highest tensile strength (Gosline *et al.*, 1999; Pérez-Rigueiro *et al.*, 2001). Its properties are due to the glands, which produce the fibre proteins, the silk composition and the fibre, which is determined by the spinning process (Dai *et al.,* 2003).

One group at the Technical University of Munich has found a solution for the production of artificial dragline spiders silk in large quantities. The group of Dr. Thomas Scheibel transferred a spider silk production gene into bacteria. The so "infected" bacteria start the production of "artificial" spider silk proteins. These proteins can be used for the fabrication of

silk filaments. Huemmerich *et al*. (2004) could prove that the natural and the artificial spiders silk are chemically identical. What was lacking so far was a proof that also the mechanical behaviour of the two silks is similar. The newly developed *in situ* testing method was used for the mechanical investigations of both types of silk fibres. Due to the influence of humidity on the behaviour of the spiders silk, the dry state achieved in the vacuum chamber of the FIB system was advantageous for the mechanical tests. It provides a reference state for all tests which is quickly and reproducibly achieved.

Tensile tests on natural and artificial spider silk

For testing, 10 mm long spider silk fibres of each of the silks were glued between two metal blocks using carbon adhesive pads. The micromanipulator was brought into contact with the silk. Using tungsten deposition, it was possible to glue the silk fibres onto the AFM tip (Figure 3.14).

They were cut free near the AFM tip at one end, leaving an 80µm long free-standing fibre at the other, which was fixed with tungsten tapes onto a metal block for testing, following the procedure described in Chapter 2.3.2. Figures 3.15, 3.16 and 3.17 show the spider silk fibres before (a) and after (b) the tensile tests.

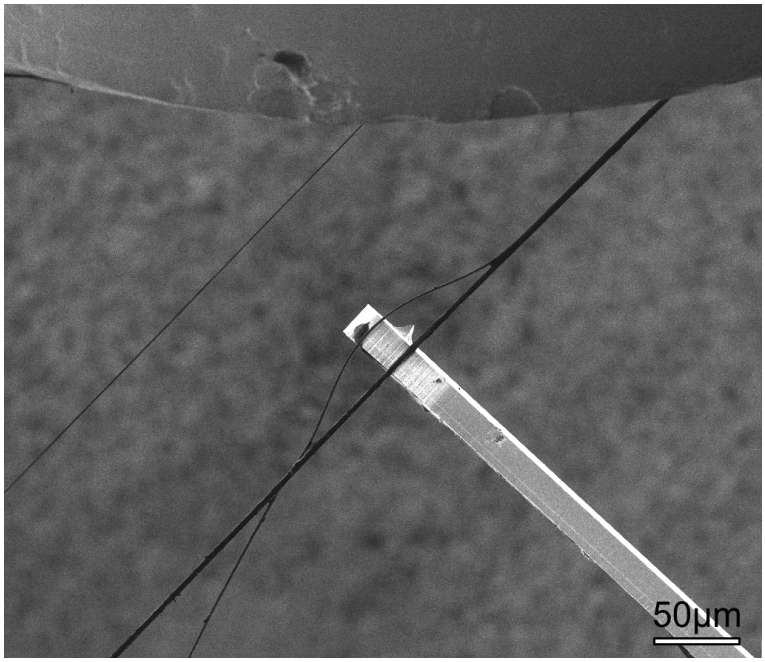

Figure 3.14: AFM tip in contact with the silk fibres (FIB micrographs).

After the test, the cross-sectional area was calculated twice from cross-sections cut with the FIB at regular intervals along the fibre, as described in Chapter 2.7. For the first calculation of the cross-sectional area, only the outer contour of the sample was taken into account, estimating a fully dense sample. For the second calculation of the cross-sectional areas, the areas of the pores were subtracted and the porosity was calculated.

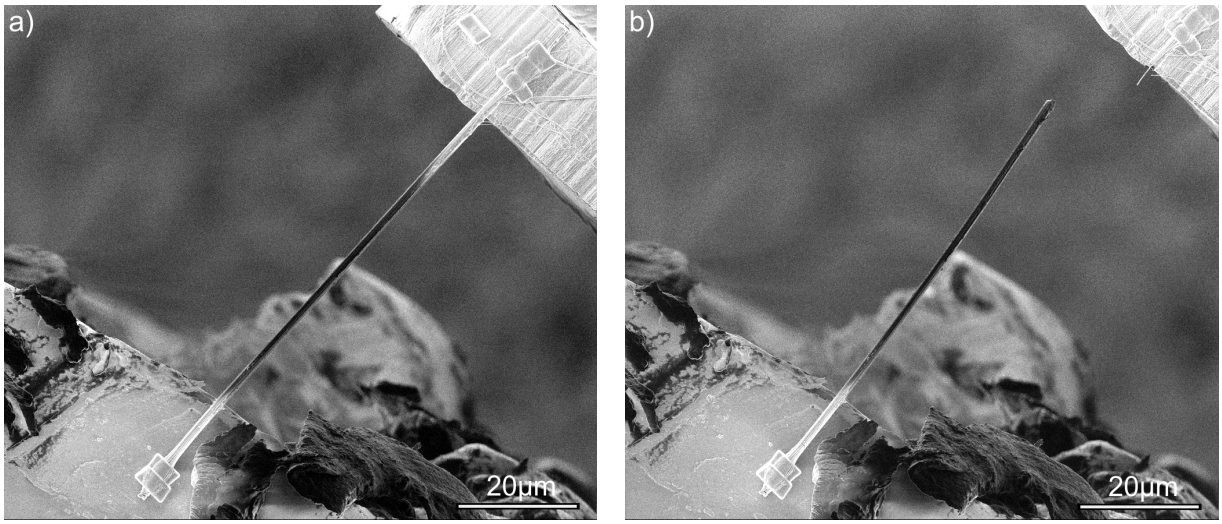

Figure 3.15: a) Natural spider silk fibre glued between the AFM tip (upper right) and the supporting metal block (lower left). b) Ruptured silk fibre after the tensile test (FIB micrographs).

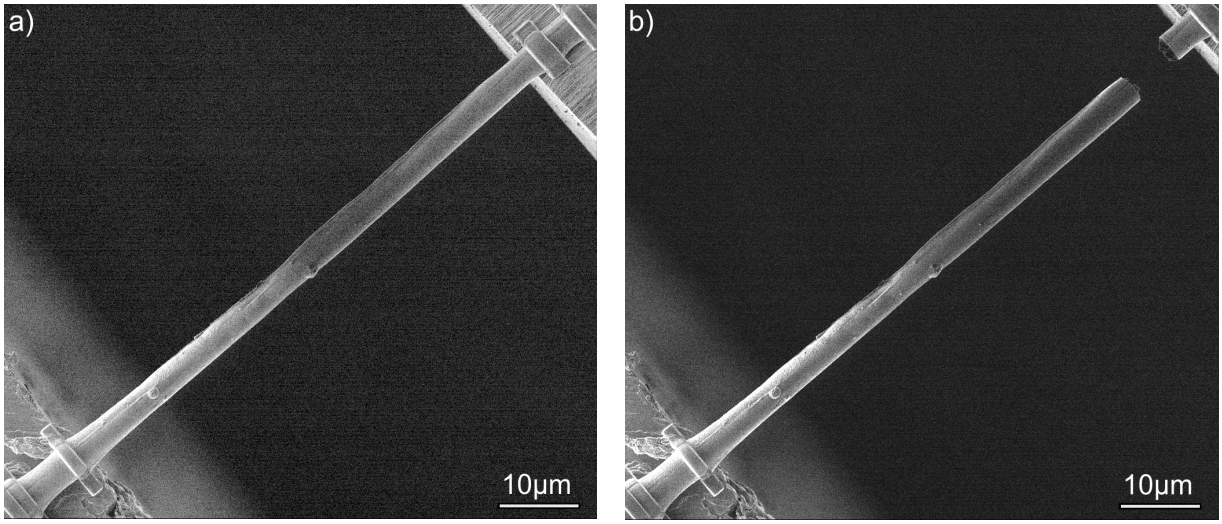

Figure 3.16: a) Sample 1 of the artificial spider silk fibre glued between the AFM tip (upper right) and the supporting metal block (lower left), ready for testing. b) Ruptured sample after the tensile test (FIB micrographs).

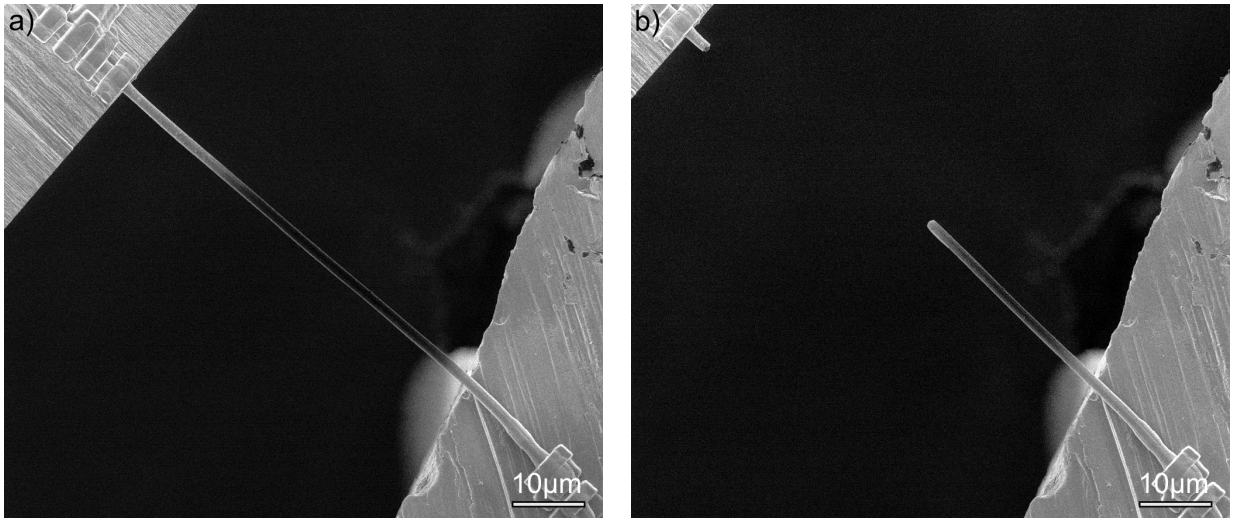

Figure 3.17: a) Sample 2 of the artificial spider silk fibre glued between the AFM tip (upper right) and the supporting metal block (lower left), ready for testing. b) Ruptured sample after the tensile test (FIB micrographs).

Figure 3.18 shows the ruptured end (a) and three micrographs (b-d) of FIB prepared cross-sections of the natural silk. The natural fibre was composed of two fibrils and had a solid cross-section while the artificial silks both had a porous structure. Figures 3.19 and 3.20 show the same for the artificial fibres. Table 3.5 lists the mean cross-sectional areas, estimating a dense material and subtracting the area of the pores, as well as the porosity of the fibre.

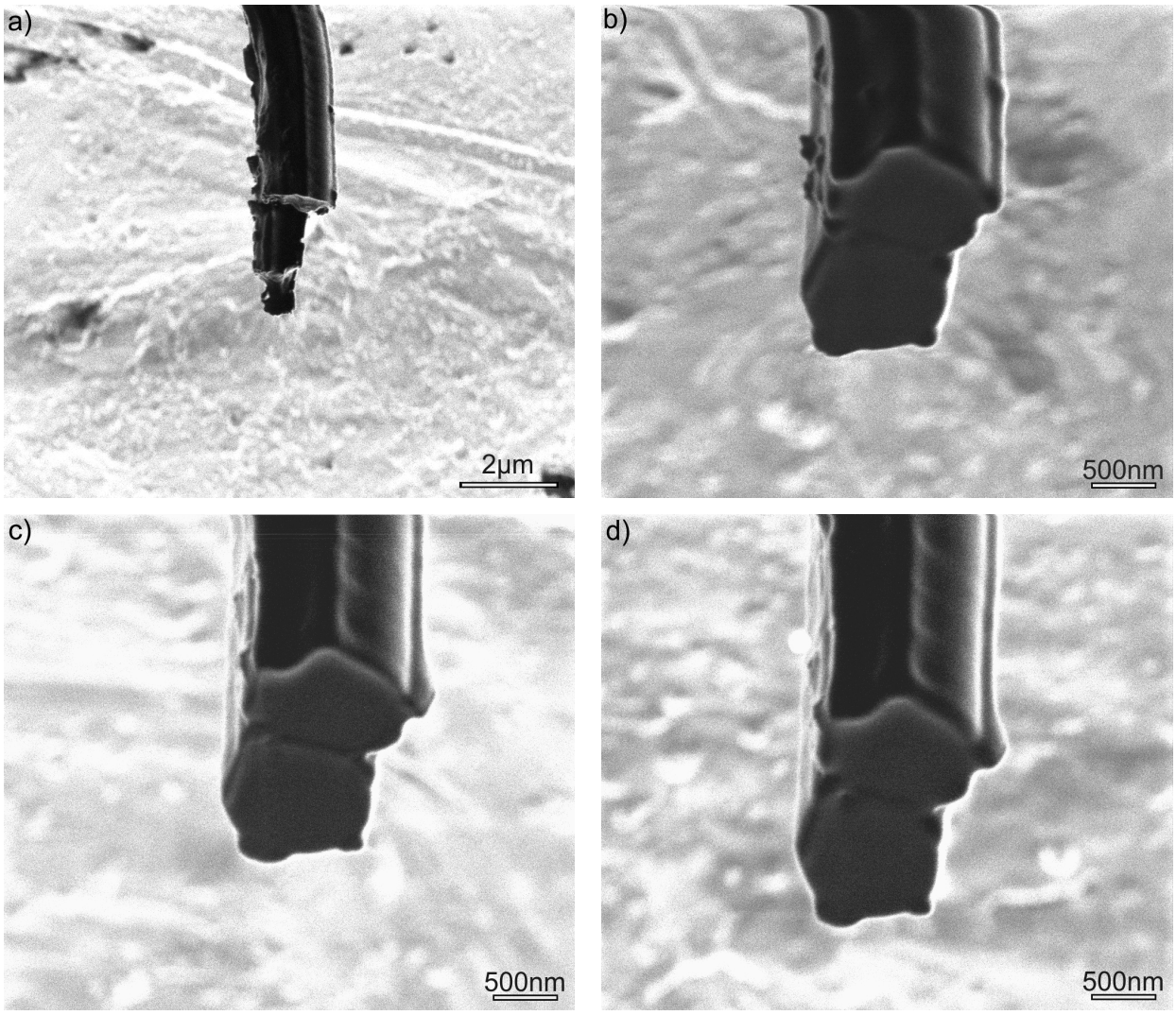

Figure 3.18: a) Ruptured end of the natural spiders silk. b)-d) Three cross-sections, showing that the silk fibre tested consisted of two filaments. The mean cross-sectional area of the fibre was 2.52±0.10 µm² (FIB micrographs, milling parameters: beam current = 150 pA (milling), 11 pA (cleaning), dwell time = 1.0 µs, overlap = 50 %).

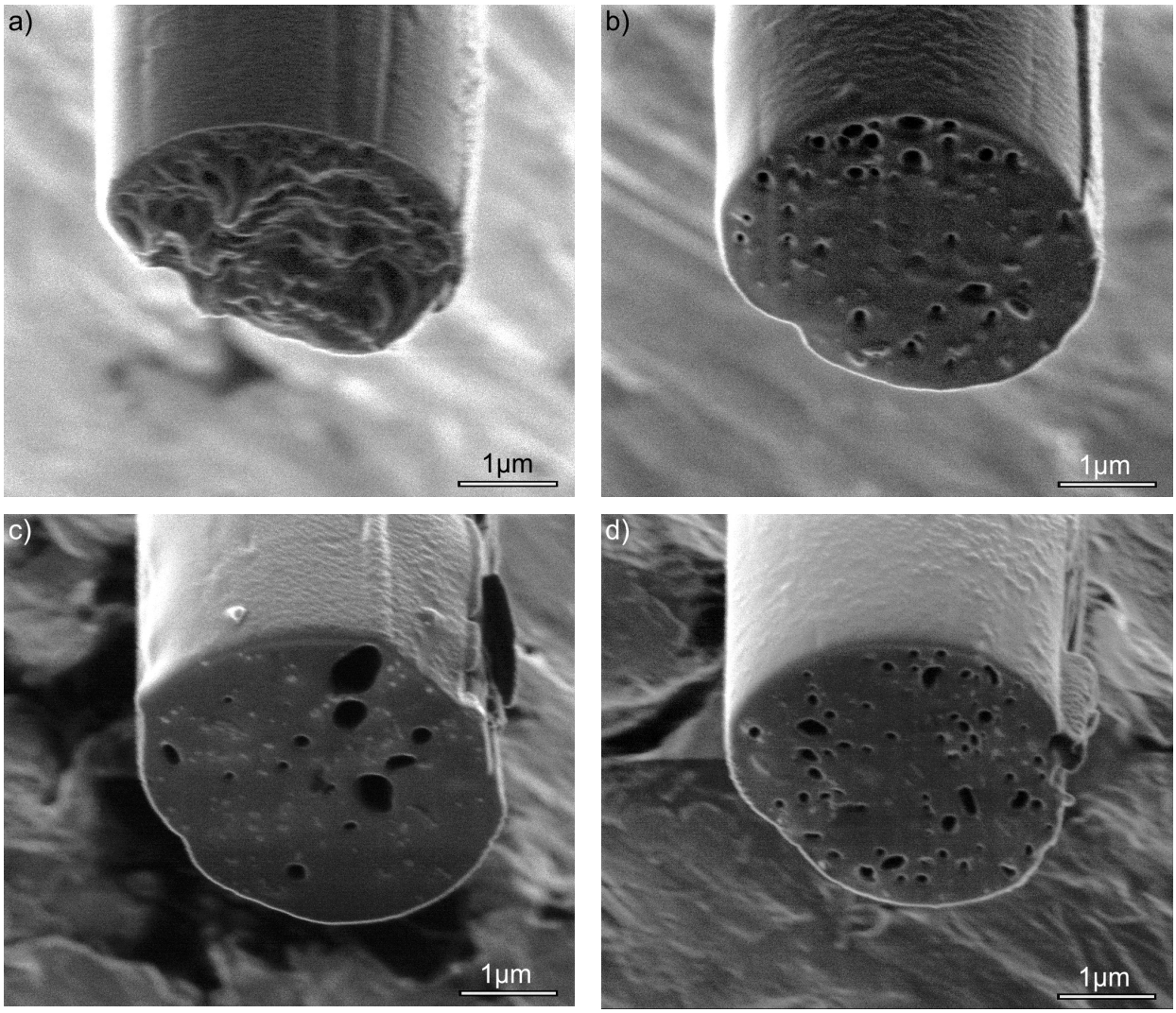

Figure 3.19: a) Ruptured end and b) – c) cross-sections cut using the FIB of Sample 1 of the artificial spider silk. The mean cross-sectional is 12.1±1.3 µm² estimating a dense material and 11.6±1.5 µm² subtracting the area of the pores (FIB micrographs, milling parameters: beam current = 150 pA (milling), 11 pA (cleaning), dwell time = 1.0 µs, overlap = 50 %).

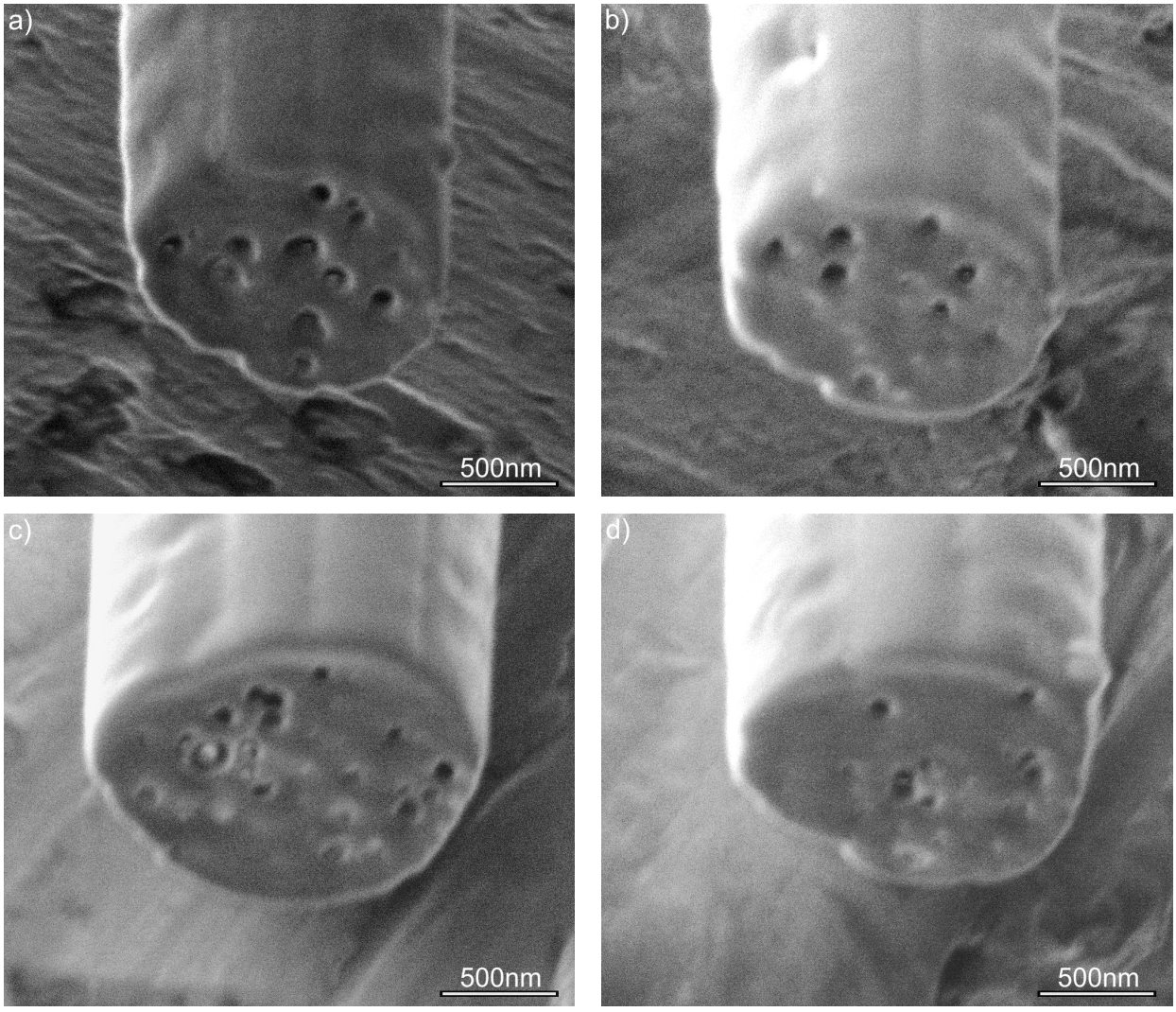

Figure 3.20: Cross-sections cut using the FIB of Sample 2 of the artificial spider silk. The mean cross-sectional area is 1.7±0.4µm² estimating a dense material and 1.6±0.4 µm² subtracting the area of the pores (FIB micrographs, milling parameters: beam current = 150 pA (milling), 11 pA (cleaning), dwell time = 1.0 µs, overlap = 50 %).

Table 3.5: Mean cross-sectional areas and porosities obtained from the FIB micrographs for the natural and the artificial silk fibres.

Material	Cross-sectional area, assuming 0 % porosity (dense material) [µm²]	Cross-sectional area, subtracting the area of the pores [µm²]	Porosity [%]
Natural Silk	2.52±0.10	—	—
Artificial Silk Sample 1	12.1±1.3	11.6±1.5	4.7±1.9
Artificial Silk Sample 2	1.7±0.4	1.6±0.4	2.8±0.4

The strain was measured from micrographs, as described in Chapter 2.6. The stress was calculated by dividing the measured force by the mean cross-sectional area. Figures 3.21 and 3.22 show the stress-strain curves for natural and artificial silk calculated using the cross-sectional areas estimating a dense material. That the two filaments broke one after another can be seen in Figure 3.21.

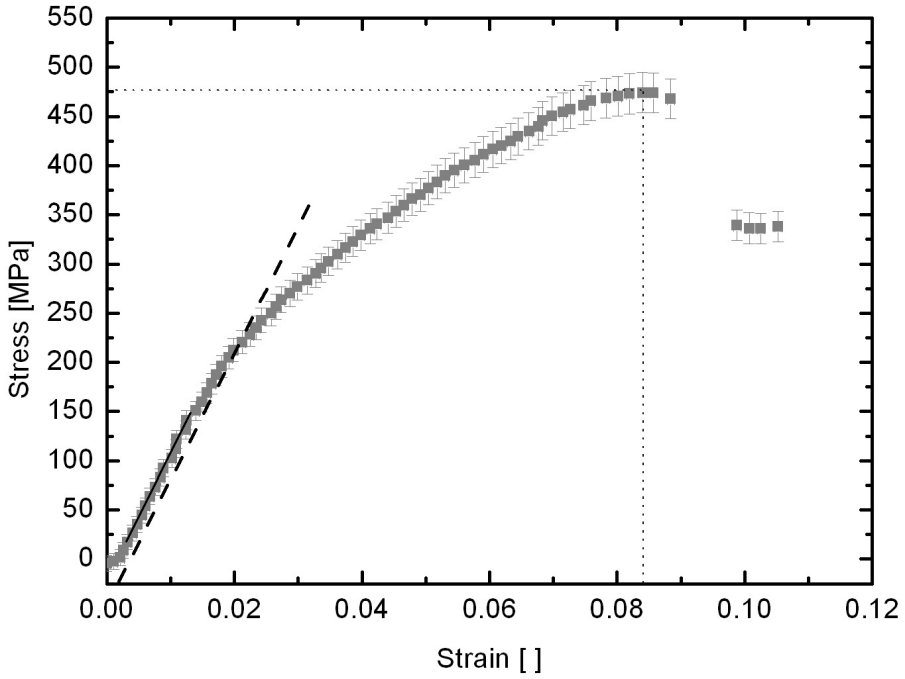

Figure 3.21: Stress - strain plot of natural spider silk. The dashed line marks the 0.2 % proof stress.

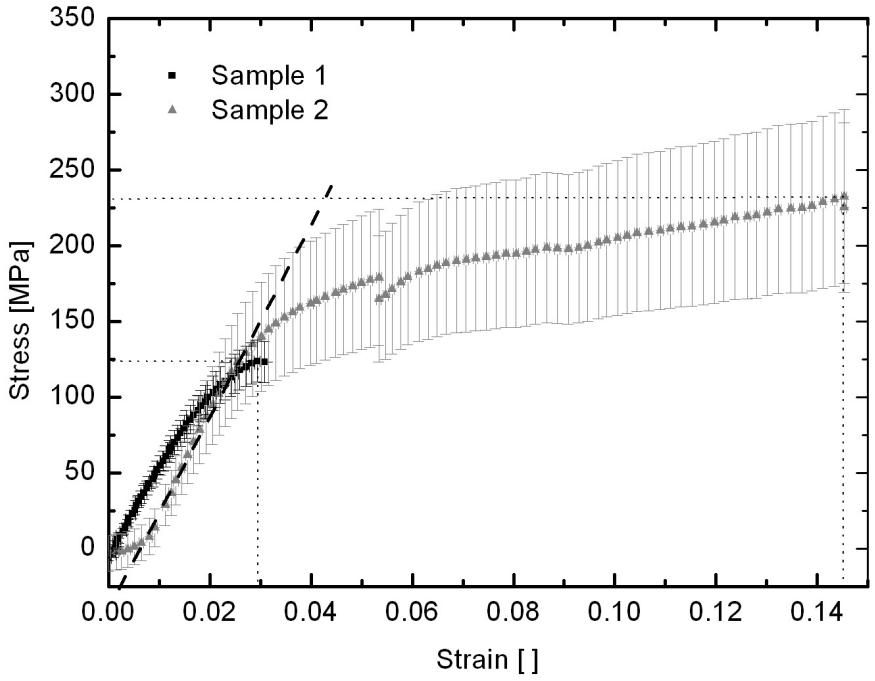

Figure 3.22: Stress - strain plot for the two samples of the two artificially made spider silks. Sample 1 was the thicker sample with a higher porosity than Sample 2, which was thinner. The dashed line marks the 0.2 % proof stress.

The slopes of all samples can be divided into three regions. At first, the samples had to be tightened and a bulge was removed, which was induced by a thermal motion of the setup during sample preparation. The second region is characterised by a linear elastic behaviour and the third dominated by plastic deformation. The Young's modulus was calculated from fitting a straight line to the slope of the linear elastic region shown in Figure 3.23 as a "zoom in" of Figure 3.22 (error calculation in Appendix 6.3).

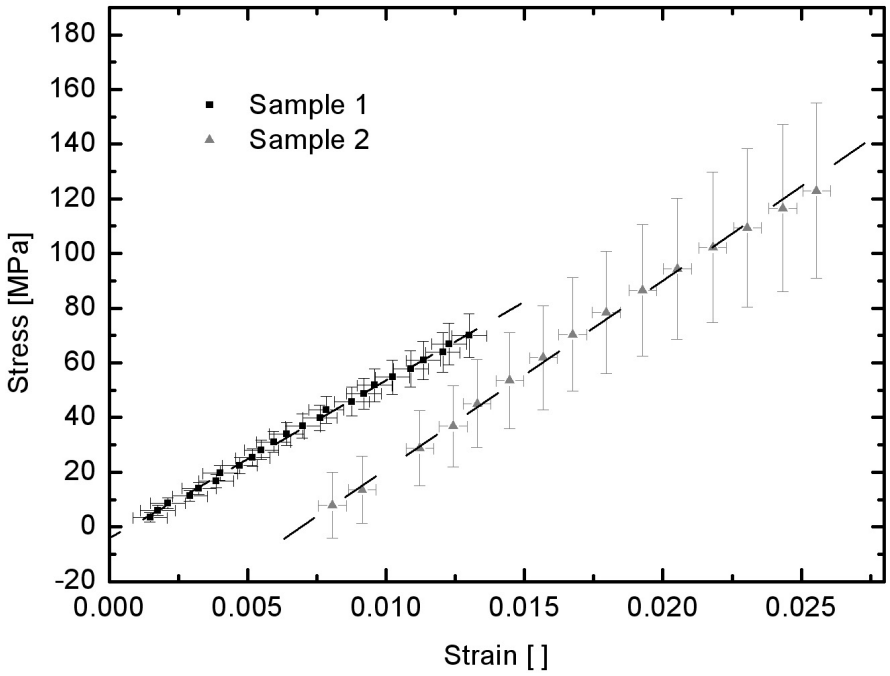

Figure 3.23: "Zoom in" of Figure 3.22 showing the linear elastic region of the two stress-strain plots from which the Young's modulus of the artificial spiders silks Sample 1 and Sample 2 was calculated.

Table 3.6 lists the measured Young's modulus, tensile strength and strain to failure for all samples, calculated with the two cross-sectional areas of fully dense material and with the pores subtracted.

Table 3.6: Young's modulus of the spider silk fibres determined from the linear regimes of the curves, their tensile strengths and strains to failure.

Material	Young's modulus, assuming dense material [GPa]	Young's modulus, porous material [GPa]	Tensile strength, assuming dense material [MPa]	Tensile strength, porous material [MPa]	0.2 % proof stress, assuming dense material [MPa]	Strain to failure [%]	Strain rate [nm/s]
Natural Silk	11.5±1.0	—	474±20	—	214.3	8.84±0.06	5.3
Artificial Silk 1	5.8±0.3	6.1±0.3	124±14	130±17	110.8	2.94±0.06	27.9
Artificial Silk 2	6.9±1.4	7.1±1.4	232±58	239±58	127.6	14.53±0.05	7.0

Figure 3.24 shows a comparison of the mechanical behaviour of the artificial (estimating a dense Sample 1 and 2) and natural spider silk fibres.

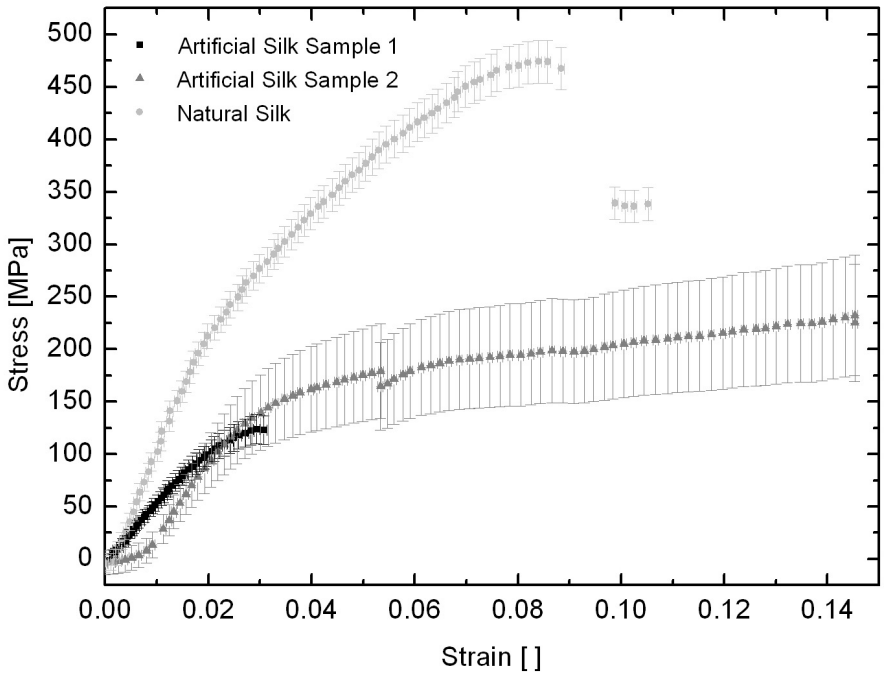

Figure 3.24: Slopes of the tested silk fibres compared.

The comparison of the three different silk fibres tested (Figure 3.24) shows that the Young's modulus and the tensile strength of the natural spider silk is nearly twice as high as those of the artificial spider silk samples.

3.3.3 Mechanoreceptor properties:
A filiform airflow sensor on crickets (*Acheta domesticus*)

The hair-like filiform sensors found on the cerci of crickets, cockroaches and other insects are examples for mechanoreceptors which are sensitive to touch, airflow and sound, gravity and the deformation of the exoskeleton (Kiel, 1998). The filiform sensors serve as antennae for these stimuli and transfers mechanical stimulation to sensory cells positioned directly underneath them in the cuticle.

The structure of filiform sensors found on the cerci of the cricket (*Acheta domesticus*) was described in Chapter 1.4.2. The interest in filiform sensors is not only for a better understanding of their structure from a biological point of view, but also for their mechano-electrical function in the hope that technical sensors inspired by these can be developed. Part of the research efforts in this area are simulations of both a single filiform sensor and an array of filiform sensors. For such experiments, an exact knowledge of the mechanical behaviour of the wind-receptor hairs is required. So far, the Young's modulus and the tensile strength of the wind-receptor hairs were unknown (Kumagai *et al.*, 1998). Due to the size and geometry of the filiform sensors, the newly developed *in situ* testing method was ideal to perform tensile tests on individual wind-receptor hairs.

Specimens were prepared from crickets (*Acheta domesticus*) which had been stored in ethanol. The cerci of one cricket was cut and, after drying, a number of the filiform sensor hairs were removed and glued onto a small metal block with carbon adhesive pads with the tapered end free. Once inside the FIB system, the hairs were affixed onto the AFM tip using tungsten tapes (Figure 3.25).

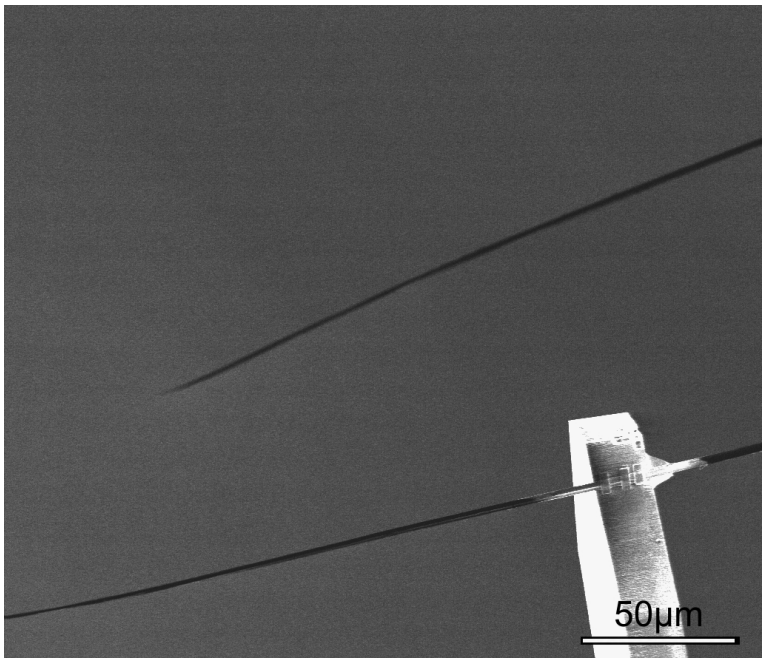

Figure 3.25: A wind-receptor hair of the filiform sensor found on the cerci of crickets fixed to the AFM tip using tungsten tapes (FIB micrograph).

The hairs were one by one cut free at their base and the free end moved onto the metal block, where they were affixed with tungsten tapes as well. The tensile tests were performed as described above in Chapter 2.5. Figures 3.26 and 3.27 show a) a wind-receptor hair glued between the AFM tip and the supporting metal block ready for testing, and b) the ruptured samples after testing Sample 1 and Sample 2, respectively.

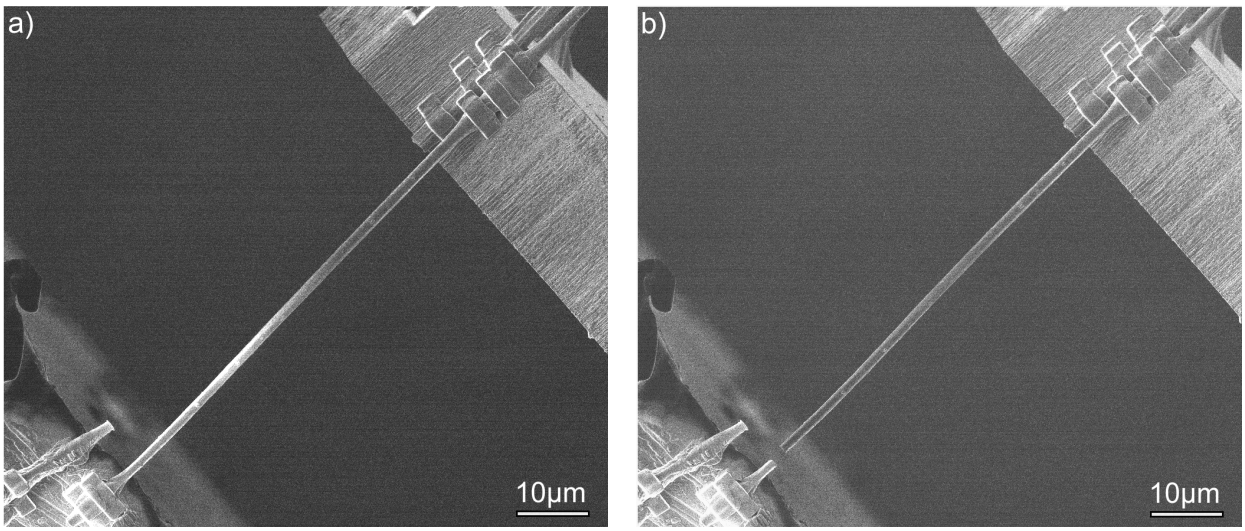

Figure 3.26: Sample 1. a) Wind-receptor hair of the filiform sensor glued with one end onto the AFM tip (upper right) and with the opposite tapered end onto the metal block (lower left). b) Ruptured sensor hair after the tensile test (FIB micrographs).

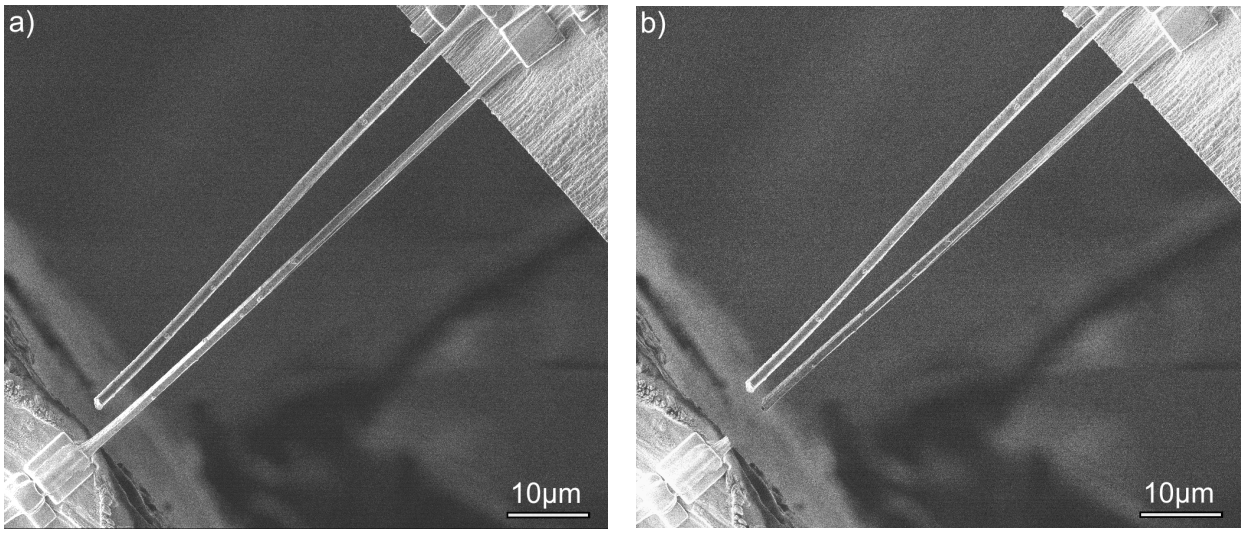

Figure 3.27: Sample 2. a) Wind-receptor hair of the filiform sensor glued with one end onto the AFM tip (upper right) and with the opposite tapered end onto the metal block (lower left). b) Ruptured sensor hair after the tensile test (FIB micrographs).

After the tensile tests, cross-sections were cut at regular distances along the two wind-receptor hairs using the FIB system. From the micrographs of the cross-sections, a mean cross-sectional area was calculated (Chapter 2.7). Since the filiform sensors exhibited porosity, one cross-sectional area was calculated estimating a dense material (neglecting the pores), using only the outer diameter, while the second cross-sectional area was calculated subtracting the area of the pores. Figures 3.28 and 3.29 show the cross-sections of Sample 1 and Sample 2, respectively.

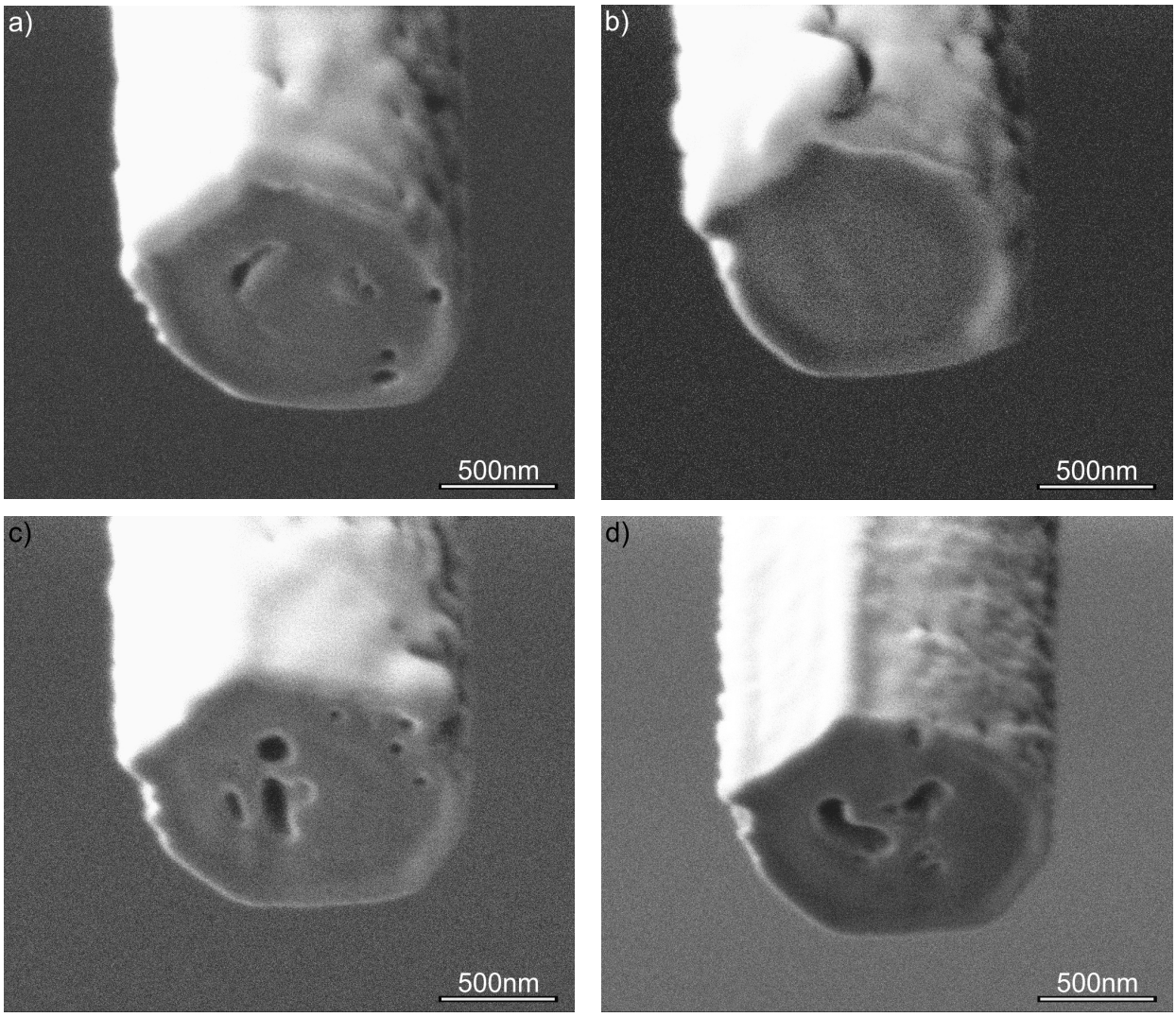

Figure 3.28: Sample 1. Cross-sections of the wind-receptor hair tested in the first test. The mean cross-sectional area is 1.56±0.22 µm² neglecting the pores and 1.50±0.26 µm² subtracting the area of the pores (FIB micrographs, milling parameters: beam current = 150 pA for milling, 11 pA for cleaning, dwell time = 1.0 µs, overlap = 50 %).

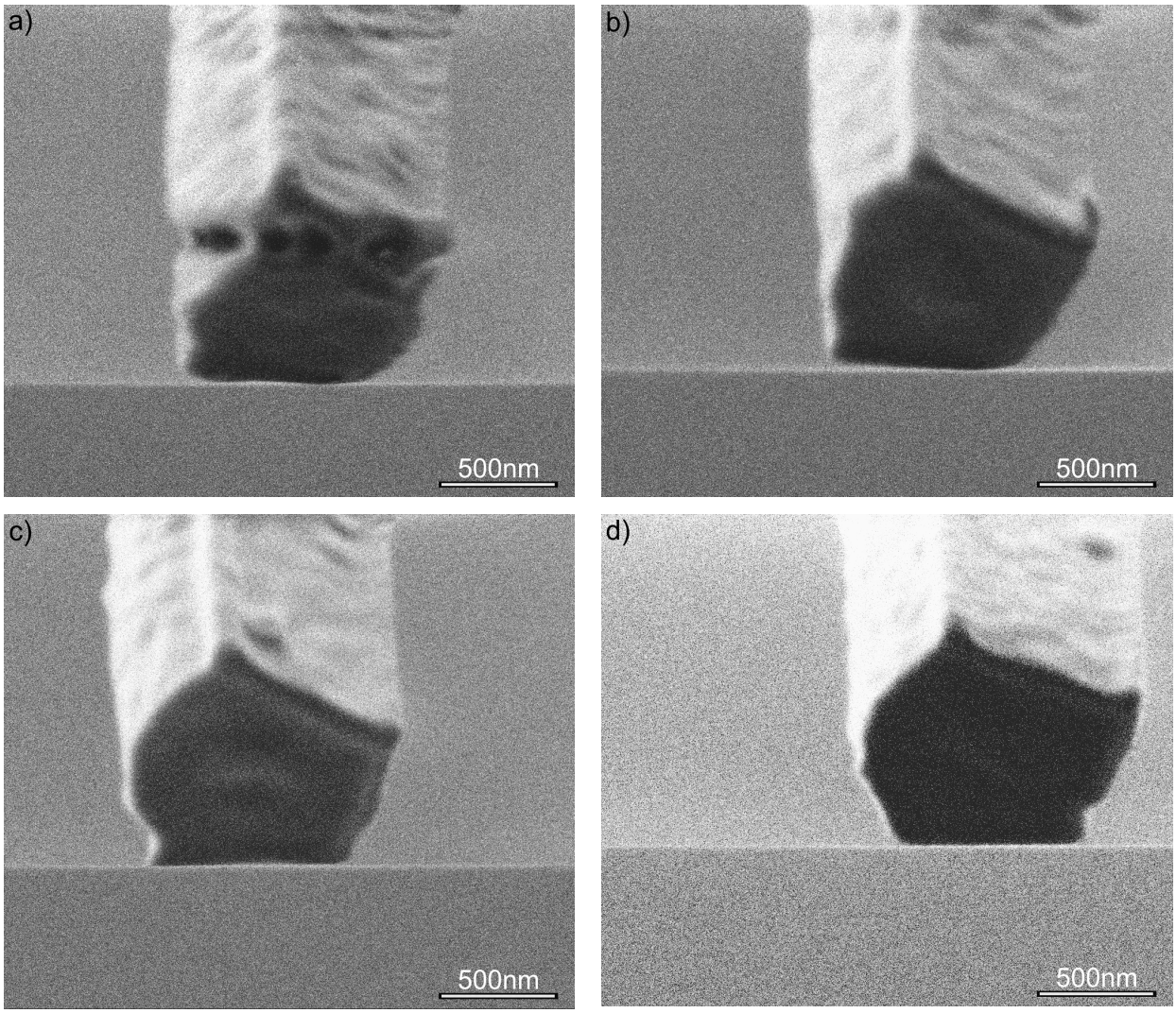

Figure 3.29: Sample 2. Cross-sections of the wind-receptor hair tested in the second test. The mean cross-sectional area is 1.10 ± 0.14 μm² neglecting the pores and 1.08 ± 0.17 μm² subtracting the area of the pores (FIB micrographs, milling parameters: beam current = 150 pA for milling, 11 pA for cleaning, dwell time = 1.0 μs, overlap = 50 %).

Table 3.7 lists the cross-sectional areas and the porosity of the two samples.

Table 3.7: Mean cross-sectional areas and porosities of Sample 1 and Sample 2 obtained from the FIB micrographs.

Sample	Cross-sectional area, assuming 0 % porosity (dense material) [μm²]	Cross-sectional area, subtracting the area of the pores [μm²]	Porosity [%]
Filiform sensor Sample 1	1.56±0.22	1.50±0.26	3.7±28
Filiform sensor Sample 2	1.10±0.14	1.08±0.17	1.6±2.1

For both samples, the strain was measured from the micrographs taken during the tensile tests as described in Chapter 2.6. The stress was calculated dividing the force by the mean cross-sectional area. Combining the results, stress-strain curves could be plotted (error calculation in Appendix 6.3). Figure 3.30 shows the stress-strain curves calculated for the cross-sectional areas assuming fully dense samples.

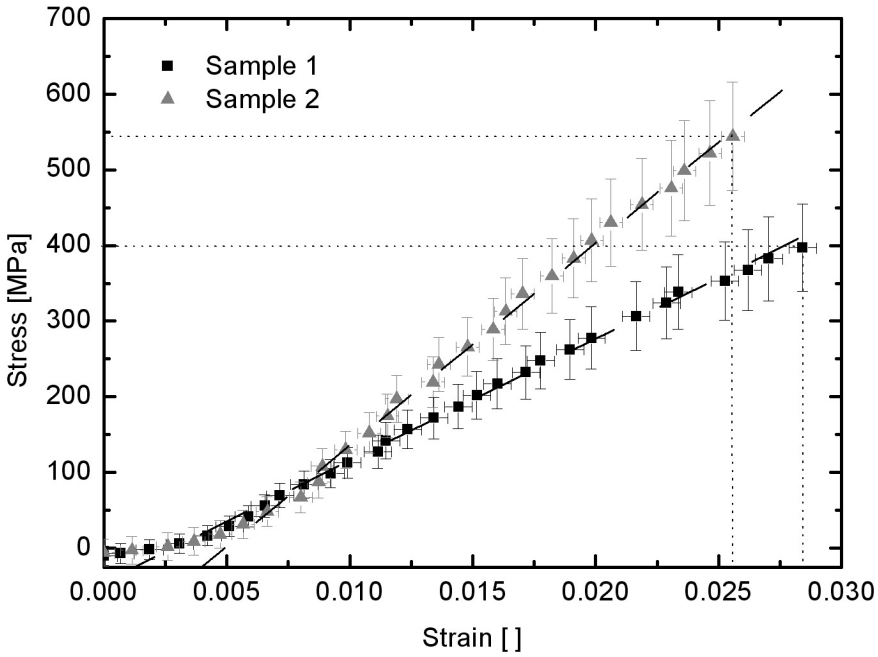

Figure 3.30: Stress-strain plot for the two wind-receptor hairs of the filiform sensors (Sample 1 and Sample 2), from the cerci of a cricket (*Acheta domesticus*).

Both samples showed linear elastic behaviour after a short regime in which a bulge in the sample was overcome and the sample was straightened. Table 3.8 lists the mechanical properties of both samples calculated for the mean cross-sectional areas, neglecting first the pores and then subtracting the pores.

Table 3.8: Mechanical properties of the wind-receptor hairs of the filiform sensors (Sample 1 and Sample 2), from the cerci of a cricket (*Acheta domesticus*).

Material	Young's modulus, assuming dense material [GPa]	Young's modulus, pores subtracted [GPa]	Tensile strength, assuming dense material [MPa]	Tensile strength, pores subtracted [MPa]	Strain to failure [%]	Strain rate [nm/s]
Filiform sensor Sample 1	16.3±1.2	17.0±1.5	396±55	411±73	2.84±0.06	4.1
Filiform sensor Sample 2	27.6±2.2	28.1±1.9	544±72	552±89	2.56±0.05	4.1

3.4 Discussion

Tests both in bending and in tension were carried out on a range of micrometer scale polymeric and biological materials to illustrate the versatility of the *in situ* mechanical testing method developed in Chapter 2. Below, their mechanical properties and mechanical performance are discussed with reference to literature values.

3.4.1 Bending tests

The first mechanical tests performed with the new testing method were beam bending tests. The advantage of cantilever bending experiments is that sample preparation and mounting of the sample is sometimes easier when compared with that required for tensile testing.

Kapton®

The Young's modulus of the polymer Kapton® was the first to be characterised in bending experiments to prove the accuracy of the *in situ* testing device.

Table 3.9: Measured mechanical properties of the Kapton® sample.

Sample tested	Testing mode	Young's modulus (loading) [GPa]	Young's modulus (unloading) [GPa]
Kapton®	Bending	3.73±0.60	3.60±0.54
Kapton®	Nanoindentation (continuous stiffness measurement)		3.48±0.08

The results from tests on 8 different positions along a FIB micromachined, 13.1 µm thick cantilever agrees with that obtained by 40 nanoindentation tests (continuous stiffness measurements) at an indentation depth of 500 nm on 125 µm thick Kapton® sheets from the same manufacturer (Table 3.9). Thus the *in situ* testing device produces correct and reliable results. The standard deviation of the bending measurements shows further that the measurements are reproducible.

Horse hair

Bending experiments on horse hair show that the testing method is well suited for the measurement of fibres and fibre-like samples. Table 3.10 lists the results obtained *in situ* and literature values for comparison.

Table 3.10: Measured mechanical properties of the horse hair sample and literature values:

Sample tested	Testing mode	Young's modulus (loading) [GPa]	Young's modulus (unloading) [GPa]	Reference
Horse hair (vacuum dry)	Bending	6.28±0.66	6.37±0.64	
Horse hair (air dry)	Tension	7.0±0.5		Pitteroff and Woodhouse (1998)
Horse hair	Acoustical waves	7.0		Pitteroff and Woodhouse (1998)
Horse hair	Vibration	9.0±1.5		Pitteroff and Woodhouse (1998)

Literature values for the mechanical properties of horse hair are rare. Pitteroff and Woodhouse (1998) measured the Young's modulus of single horse hairs from violin bows in tension, with acoustical waves and in vibrational tests (Table 3.10). The *in situ* value agrees well with theirs, particularly considering that bending measurements tend to be about 10% lower than tensile due to shear effects and that vibrational measurements typically yield a higher modulus than those obtained by static mechanical testing. Other factors which, in addition to the different testing methods, influence the mechanical properties of horse hair are differences between species, the horse's gender and individual horses, as well as variations between individual hairs and even along the length of an individual hair, where they vary from the freshly grown base to the older hair at the tip (Pitteroff and Woodhouse, 1998). The moisture content of the hair seems to have only a moderate effect on its properties. The values measured in bending in the SEM (dry, in vacuum) differ only slightly from those of Pitteroff and Woodhouse (1998) who tested the horse hair in air.

Spruce wood

Measurements of the Young's modulus of spruce (*Picea sp.*) cell wall material cut from mid-year tracheids show the strength of the testing method for the investigation of structured materials. Sample preparation was eased by the use of the FIB system which allows to prepare

samples from individual structural components at a length scale which otherwise are hardly, if at all, accessible for testing. This fact is also reflected by the relatively small number of mechanical tests on individual wood cell wall samples reported in the literature. Table 3.11 lists the results of the *in situ* tests described in Chapter 3.2.3 on a cell wall cantilever cut from a spruce tracheid and literature values for comparison.

Table 3.11: Measured mechanical properties of the spruce wood cell wall sample and literature values.

Sample tested	Testing mode	Young's modulus (loading) [GPa]	Young's modulus (unloading) GPa]	Reference
Spruce wood cell (vacuum dry)	Bending	28.2±4.0	25.6±4.0	
Norway spruce wood cell (*Picea abies*) (air dry)	Nanoindentation	6.9 to 18.8		Gindl *et al.* (2004)
Spruce wood cell (*Pica abies* [L.] Karst.) (dry tested at air, 65% relative humidity)	Tension			Burgert *et al.* (Part 3, 2005)
chemically obtained		20.1+5.7/-8.3		
mechanically obtained		20.1+16.7/–11.8		
Spruce wood cell (air dry)	Tension	20.4±4.7		Burgert (2005)
Spruce wood cell (wet)		15.6±3.7		

The value of the Young's modulus measured *in situ* is considerably higher than that measured by nanoindentation (Gindl *et al*., 2004), since nanoindention measures an average of the longitudinal and the transverse Young's moduli, which typically differ by one magnitude. Gindl and Schöberl (2004) state further that nanonindentation measurements also underestimate the longitudinal Young's modulus, because the wood cell walls are loaded at an angle of approximately 25° to the microfibril angle. The effect of the microfibril angle on the wood cell wall properties measured by nanoindentation is not known.

The only other measurements of the mechanical properties of individual wood cell walls comparable to those described in this thesis were reported by Burgert (2005) and Burgert *et*

al. (Part 3, 2005). They tested chemically and mechanically isolated fibres of spruce (*Picea abies* [L.] Karst.) from the transition wood zone, that is summer wood, of a 120 year old spruce tree. Their tensile tests were carried out on air-dry samples in an environment of 22°C and 65% relative humidity. While the mean of these measurements is a little lower than the *in situ* value, Burgert *et al.* (Part 3, 2005) show much higher Young's moduli than those of the *in situ* test measured in some samples and remarkable scatter in values.

A number of factors lead to these large variations in material properties. Wood is a composite material, which consists of cellulose fibres embedded in a lignin matrix (Dinwoody, 2000). As in any other fibre-composite, the fibre content, here cellulose microfibrils, influences the mechanical performance of the wood cell wall. Also the microfibril angle (tilt angle of the cellulose fibrils with respect to the longitudinal cell axis) in the wood cell wall plays an important role: the smaller the microfibril angle, the larger the Young's modulus of the wood cell wall (Gindl *et al.*, 2004). Similarly important is the moisture content of the wood. Burgert (2005) shows that the Young's modulus increases by 30% on drying the wood cell wall from fresh (30% moisture content) to air-dry (12% moisture content). In vacuum, the moisture content can be assumed close to 0%, the *in situ* measurements can thus be expected to be higher, for the same microfibril angle. Niemz (1993) describes that a moisture content of 30 %, which is the fibre saturation point where the wood cell walls hold the maximum amount of bound water, corresponds to a Young's modulus of 70 % of the value for 0 % moisture content (Young's modulus 100 %). Using the values of Burgert (2005) for wet (moisture content 30 %) spruce wood (Young's modulus 15.6±3.7 GPa = 70 % the Young's modulus for 0 % moisture content, according to Niemz, 1993), one can calculate the theoretical Young's modulus for 0 % moisture content to be about 22.3 GPa which is in the range of the values measured with the new *in situ* testing method (Table 3.11).

An interesting observation made during sample preparation was that the wood cell wall cantilever started to twist once it was cut free in the FIB. Burgert *et al.* (Part 2, 2005) report the same. The twisting of the fibres was found to be correlated to their moisture content and the microfibril angle in the cell wall: oven (or vacuum) dry cells twisted more than air-dry ones, and the maximal twist was observed at a microfibril angle of 45°. Burgert *et al.* (Part 2, 2005) suggest that the anti-clockwise rotation of the cell wall is due to an anisotropic shrinkage of the cell wall because of the helical arrangement of the cellulose microfibrils in the S2 layer.

3.4.2 Tensile tests

The advantage of tensile tests over tests in bending is that the mechanical properties, also of composite materials or samples with a complex geometry, are easily accessible. With tensile tests, the Young's modulus, tensile strength and strain to failure of a material can be determined, not only the Young's modulus as it is the case in bending tests on cantilevers. The results of tensile tests on a number of different materials and structures are discussed below.

The samples tested in tension broke close to the tungsten tapes and, except of the wind-receptor hairs of the filiform sensor samples, they also broke on the end which was glued to the AFM tip. A possible explanation for this phenomenon is that the tungsten tapes, which were used for the mounting of the samples, are leading to a weakening in the sample due to the influence of the ion beam, which is discussed in detail in Chapter 1.6. However, in the case of the seta and the wind-receptor hairs, the samples were slightly tapered to the end which broke, thus also geometrical factors need to be considered. Further investigations on the influence of the sample during mounting are required in order to analyse, if the sample was weakened during mounting and if the influence on the sample can be minimised by using lower beam currents for the tungsten deposition, for example.

For the spider silk and filiform samples which showed a porosity, only the values of the mechanical properties of the dense material, calculated using the outer diameter of the sample (without subtracting the areas of the pores), will be discussed, for two reasons: (i) the influence of the porosity falls within the error for the calculation of the mechanical properties and (ii) the structure and the distribution of the pores is not known, existing models for the calculation of the mechanical properties of porous materials could therefore not be applied.

Seta of *Gastrophysa viridula*

The present testing method is unique in that, to date, it is the only one with the necessary force, strain range and resolution for tensile testing of a single seta. Table 3.12 lists the results from the *in situ* tests and literature values from nanoindentation for comparison.

Table 3.12: Measured mechanical properties of the single seta of the beetle *Gastrophysa viridula* and literature values for comparison.

Sample tested	Testing mode	Young's modulus [GPa]	Tensile strength [MPa]	Strain to failure [%]	Reference
Beetle seta *Gastrophysa viridula*	Tension	11.2±1.0	309±60	2.51±0.06	
Beetle head *Pachnoda marginata*	Nano-indentation	7.50±1.80 (dry) 1.50±0.80 (fresh)			Barbakadze (2005)
Tanned insect cuticle (highly cross-linked)		10 to 25			Vincent and Wegst (2004)

The Young's modulus of the seta of the beetle *Gastrophysa viridula* falls in the typical range of that of dry, tanned (highly cross-linked) insect cuticle (Vincent and Wegst, 2004). The high Young's modulus of setae is thought to be beneficial to the insect's attachment performance and allows the hair-like structures to be more densely packed without sticking together (Spolenak *et al.,* 2005). The seta requires a high strength to prevent rupture under stress. This strength and the high Young's modulus are probably due to an alignment of the chitin fibres along the length of the individual seta.

The tensile test was performed on a dry mounted sample. The influence of the humidity on the mechanical properties of insect cuticle is significant. Typically the Young's modulus of the dry, tanned insect cuticle is higher by a factor of 2 to 5 than wet, tanned insect cuticle (Vincent and Wegst, 2004; Wegst, 2004; Barbakadze, 2005).

Typical bodyweights of a *Gastrophysa viridula* beetle are in the range of 8 to 12 mg (Schuppert, 2005). Estimating a beetle walking on the ceiling with a bodyweight of 12 mg, the weight of its body will apply a tensile load to the setae in contact with the ceiling. If only one seta is in contact, the stress in the seta will be 61 MPa, which is 5 times lower than the tensile strength of the seta. One single foot of the beetle has 1500 to 2000 setae, which are not all in contact, but presumably at least 2/3 are in contact, the beetle has 6 feet, where at least 4

are in contact with the ceiling during walking, so one can calculate a rather high safety-factor of 26666 for the prevention of rupture of the setae.

Filiform sensor on crickets

The Young's modulus of two wind-receptor hairs, obtained from the filiform sensors on the cerci on the cricket *Acheta domesticus*, as the beetle seta, consists of the chitin composite insect cuticle. It was found to have an even higher Young's modulus than the seta. Table 3.12 lists the mechanical properties of the wind-receptor hairs.

Table 3.13: Measured mechanical properties of the wind-receptor hairs from a cricket (*Acheta domesticus*).

Sample tested	Testing mode	Young's modulus [GPa]	Tensile strength [MPa]	Strain to failure [%]
Filiform 1	Tension	16.3±1.2	396±55	2.84±0.06
Filiform 2	Tension	27.6±2.2	544±72	2.56±0.05

The high stiffness of the hair is presumably necessary for its mechanical stability, so that it does not buckle under its own weight, and is also advantageous for the function of these hairs, namely, to act as mechanical sensors and to detect air-flow. Slow air movements such as sound cannot be detected from hairs with low stiffness, because the hair will bend along its length rather than load the sensor at its base. Kumagai *et al.* (1998) show further that differently sized hairs are tuned to detect air movements in differed frequency ranges.

The values of the Young's moduli of the first and second sample differ significantly. One reason for this is that the samples were not only cut from hairs of different lengths, but also that they were taken from different positions along the respective hairs. Kumagai *et al.* (1998) supports this by reporting that the mechanical properties vary along the length of the hairs. Another reason is that not only the size and shape of the wind-receptor hairs vary in order to be able to detect different airflow frequencies, but also the Young's modulus of the material of which the hairs consist.

The high Young's modulus and tensile strength are probably due to a high content and straight alignment of chitin fibres along the length of the wind-receptor hairs. However, the fibre content and orientation of the wind-receptor hairs are not known.

The samples were tested in a dry state, which also affects the mechanical properties of the insect cuticle, as discussed above for the seta of the beetle *Gastrophysa viridula*. Further investigations on the amount and orientation of the chitin fibres, as well as on the influence of the humidity on the sample behaviour are required in order to explain the high values for the Young's moduli.

Spider silk

Mechanical tests on spider silk were performed during this thesis in order to compare the mechanical properties of natural silk threads, obtained from the drag line of *Araneus diadematus* by forced silking, with those of artificially produced ones. The present testing method was found to be ideal as a reference testing method for this material.

The mechanical properties of natural and artificial spider silk tested as part of this thesis and literature values of drag line threads are listed in Table 3.14.

Table 3.14: Measured mechanical properties of natural dragline of *Araneus diadematus,* artificial silk fibres and literature values of drag line threads for comparison.

Sample tested	Young's modulus [GPa]	Tensile strength [MPa]	Strain to failure [%]	Reference
Natural spider silk (*Araneus diadematus*)	11.5±1.0 (vacuum)	474±20 (vacuum)	8.84±0.06 (vacuum)	
Artificial silk 1	5.8±0.3 (vacuum)	124±14 (vacuum)	2.94±0.06 (vacuum)	
Artificial silk 2	6.9±1.4 (vacuum)	232±58 (vacuum)	14.53±0.05 (vacuum)	
Araneus diadematus	6.5±0.3 (air dry) 1.6±0.3 (in water)	800±90 (air dry) 500±60 (in water)	22.1±2.0 (air dry) 24.9±2.8 (in water)	Shao and Vollrath (1999)
Araneus diadematus	10 (air dry)	1100 (air dry)	27 (air dry)	Gosline *et al.* (1999)
Nephila clavipes	12.71 (air dry)	850 (air dry)	20 (air dry)	Ko and Jovicic (2004)
Argiope aurentia	34 (air dry)	1750 (air dry)	36 (air dry)	Ko and Jovicic (2004)
Argiope trifasciata	6.9±0.4 (air dry)	600±50 (air dry)	30±2 (air dry)	Pérez-Rigueiro *et al.* (2001)

Natural spider silk

The natural spider silk of the *Araneus diadematus* spider showed a relatively high Young's modulus compared with the literature values of Shao and Vollrath (1999) and Gosline *et al.* (1999), whereas the tensile strength and the strain to failure were lower. This is at least partially due to the testing conditions.

A comparison of the values of the Young's modulus tested in the vacuum with literature values measured in air and in water (Shao and Vollrath, 1999) showed that all values are nearly equidistant: the Young's modulus decreases by approximately 5 GPa with increasing

moisture content from vacuum dry (the measurements presented in this thesis), to air dry and wet (values of Shao and Vollrath, 1999).

A comparison of the stress-stain curve of Figure 3.21 (silk of *Araneus diadematus* measured in vacuum) with literature values of silk from the same species of spiders (Gosline *et al.*, 1999; Vollrath, 2000) tested in air, shows the influence of water on the mechanical behaviour of spider silk. Stress-strain curves of silk tested in air showed a pronounced strain-stiffening effect, whereas in the slope of Figure 3.21 this effect is not present. Spider silk shows this behaviour only when it is exposed to water (Gosline *et al.*, 1984), or at least to the relative humidity of a laboratory.

The effect of water on spider silk is called plasticization. It reduces the interactions between the polymer chains. H-bonds between the chains are broken by the water so that chains can slide relative to one another. Table 3.14 shows that the modulus of the polymer decreases, whereas the strain to failure increases (Shao and Vollrath, 1999).

The tensile strength measured in vacuum is lower than expected from the values stated in the literature. An interesting fact is that the tensile strength obtained from the *in situ* test in the vacuum corresponds to the stress which is applied to the thread by the body mass of the spider, from which the silk was obtained. With the body mass, of the spider 122 mg = 1.2 mN, loading the cross-sectional area of the fibre 2.52±0.10 μm², corresponds to a stress of 474 MPa, which is the tensile strength measured. Thus the fibre strength is much lower than predicted by Garrido *et al.* (2002). They stated that the weight of the spider lies in the range of loads within the elastic region of the force displacement curves, of silk obtained from vertically climbing *Argiope trifasciata*. The difference is most likely due to the absence of water in the silk thread in vacuum.

Overall, a comparison of the test results with literature values of spider silk is difficult, since the values listed show large variations in the Young's modulus, tensile strength and strain to failure both for silks obtained from different individuals of the same species and even for the same individual. It is obviously a biological material which not only due to variations in moisture content, naturally shows large property ranges.

Also the speed of silk production changes the mechanical properties of the spiders silk. With increasing speed, the Young's modulus increases, the fracture strength increases and the fracture strain decreases. A fact, which has to be considered, when spider silk was obtained from forced silking, which was the case in a number of tests described in literature, as well as for the present test performed during this thesis. Also the body temperature and the spider condition affect the properties of the silk (Vollrath, 2000).

The wide experimental scatter in the measured strength values of literature data can also be explained with experimental difficulties in measuring the properties of samples with an irregular and small (2 to 5 μm in diameter) cross-sectional area accurately. The advantage of the *in situ* testing method is that the real cross-section of the spider silk can be measured with high accuracy from cross-sections prepared using the FIB system (Chapter 2.7). Investigations described in the literature used light microscopy or polarising light microscopy followed by more accurate investigations using an SEM. But even within the SEM investigations a cylindrical shape of the silk was assumed and it was believed to be constant along the whole line (Pérez-Rigueiro *et al.,* 2001). However, the shape of the silk differs from a cylindrical shape, and its diameter varies along the fibre length (5 % in natural silk, >5 % in forced silking of *Argiope trifasciata*; Pérez-Rigueiro *et al.,* 2001). The variation of the cross-sectional area of the natural silk fibre obtained by forced silking tested in Chapter 3.3.2 was 4 %.

Natural and artificial spider silk compared

The comparison of the natural and artificial spider silk showed that the artificial one reaches half the value of the Young's modulus and the tensile strength (Table 3.14) of the natural silk obtained from *Araneus diadematus*. Both were tested in vacuum. The mechanical properties of spiders silk depend on two fundamental aspects, the silk protein and the spinning of the silk (Dai *et al.,* 2003). The silk protein, which was produced by genetically modified bacteria, is chemically identical to the natural silk protein of *Araneus diadematus* as demonstrated by Huemmerich *et al.* (2004). An improvement of the mechanical properties could be achieved by modifying the method of spinning fibres from the protein solution. So far the process, how a fibre was spun from the silk proteins is unpublished.

Table 3.6 lists the strain rates of the tensile tests on natural and artificial spider silk threads. The artificial spider silk Sample 1, which was tested with the highest strain rate, shows in

Figure 3.24 (and 3.22) a smaller region of plastic deformation, a lower tensile strength and a lower strain to failure, compared to the others. So far, the influence of the strain rate on the mechanical properties of the natural and artificial spider silk is not known in detail. However, from the results in Table 3.6 one can assume that the strain rate had a significant influence on the mechanical properties of the samples tested.

The porosity of the artificial silk is too small to have a distinct influence on the mechanical properties of the samples. The porosity of the artificial silks tested (Figure 3.19 and Figure 2.20) is 4.7±1.9 % for Sample 1, and 2.8±0.4 % for Sample 2. The pores may only have an influence on the mechanical properties if their distribution is nonuniform. An agglomeration of pores can lead to a weakening of the sample at that particular point, but this phenomenon was not observed during the tests.

3.5 Conclusions

The testing method developed and described in Chapter 2, allowed the measurement of the mechanical properties of materials and structures which currently receive great research interest. The experiments showed that small scale samples can be prepared with high accuracy and that mechanical tests can be performed *in situ* in bending and tension. Tested were a single spruce wood cell in bending, a seta of the beetle *Gastrophysa viridula*, artificial spider silk fibres and the wind-receptor hairs of the filiform found on crickets. The strength of the combination of a force measuring device and a FIB system for mechanical and structural investigation of complex materials was demonstrated.

A possible problem with this dry-mount method is the presence of a vacuum during sample preparation and testing. The mechanical properties of biological materials can change considerably upon hydration. The influence of the humidity on the mechanical behaviour of each sample was discussed. In general it can be summarised that a decrease of water-content leads to an increase in the Young's modulus and tensile strength on the one hand and a decrease of the strain to failure on the other hand. The measured values will thus not represent the *in vivo* state. Further work is necessary to transfer these test methods, or similar methods to non-vacuum conditions.

3.6 References

Arzt E., Gorb S. and Spolenak R. (2003) "From micro to nano contacts in biological attachment devices" *Proceedings of the National Academy of Sciences* **100(19)**, 10603-10606

Autumn K., Liang Y.A., Hsieh S.T., Zesch W., Chan W.P., Kenny T.W., Fearing R. and Full R.J. (2000) "Adhesive force of a single gecko foot-hair" *Nature* **405**, 681-685

Autumn K., Sitti M., Liang Y.A., Peattie A.M., Hansen W.R., Sponberg S., Kenny T.W., Fearing R., Israelachvili J. N. and Full R. (2002) "Evidence for van der Waals adhesion in geko setae" *Proceedings of the National Academy of Sciences* **99**, 12252- 12256

Barbakadze N. (2005) PhD Thesis, Universität Stuttgart, Germany

Burgert I., Frühmann K., Keckes J., Fratzl P. and Stanzl-Tschegg S. (2005) "Properties of chemically and mechanically isolated fibres of spruce (*Pica abies* [L.] Karst.) Part 2: Twisting phenomena" *Holzforschung* **59**, 247-251

Burgert I., Eder M., Frühmann K., Keckes J. Fratzl P. and Stanzl-Tschegg S. (2005) "Properties of chemically and mechanically isolated fibres of spruce (*Pica abies* [L.] Karst.) Part 3: Mechanical characterisation" *Holzforschung* **59**, 354-357

Burgert I. (2005) Private communications, Max-Planck-Institute of Colloids and Interfaces, Department of Biomaterials, D-14424 Potsdam, Germany

Dai L., Zhang Y. and Ou-Yang Z. (2003) "Elastic theory of single spider silk protein molecule" *Thin Solid Films* **438-439**, 382-385

Dinwoodie J. M. (2000) *Timber: Its nature and behaviour*, 2nd edition, E & FN Spon New York, USA

Gindl W., Gupta H.S., Schöberl T., Lichtenegger H.C. and Fratzl P. (2004) "Mechanical properties of spruce wood cell walls by nanoindentation" *Applied Physics* **A 79**, 2069-2073

Gindl W. and Schöberl T. (2004) "The significance of the elastic modulus of wood cell walls obtained from nanoindentation measurements" *Composites Part* **A 35**, 1345-1349

Gnatzy W. and Schmidt K. (1971) „Die Feinstruktur der Sinneshaare auf den Cerci von Gryllus bimaculatus Deg. (Saltatoria, Gryllidae)" *Zeitschrift Zellforschung* **122**, 190-209

Goodfellow SARL, rue Solférion, F-59000 Lille, France (www.goodfellow.com → Material Properties)

Gorb S.N. (2000) *Attachment Devices of Insect Cuticle* Kluwer Academic Publishers, Dordrecht, Netherlands

Gosline J.M., Denny M.W. and DeMont M.E. (1984) "Spider silk as rubber" *Nature* **309**, 551-552

Gosline J.M., Guerette P.A., Ortlepp C.S. and Savage K.N. (1999) "The mechanical design of spider silks: From fibroin sequence to mechanical function" *The Journal of Experimental Biology* **202**, 3295-3303

Huemmerich D., Helsen C.W., Quedzuweit S., Oschmann J., Rudolph R. and Scheibel T. (2004) „Primary structure elements of spider dragline silk and their contribution to protein solubility" *Biochemistry* **43**, 13604-13612

Keil T.A. (1998) *The Structure of Integumental Mechanorezeptors Microscopic Anatomy of Invertebrates* Volume 11B Insecta pp. 385-404 Wiley-Liss, Inc.

Ko F. K. and Jovicic J. (2004) "Modeling of mechanical properties and structural design of spider web" *Biomacromolecules* **5**, 780-785

Kumagai T., Shimozawa T. and Baba Y. (1998) "The shape of wind-receptor hairs of cricket and cockroach" *Journal of Comparative Physiology* **A 183**, 187-192

Lazaris A., Arcidiacono S., Huang Y., Zhou J.-F., Duguay F., Chretien N., Welsh E.A., Soares J.W. and Karatzas C.N. (2002) "Spider silk fibers spun from soluble recombinant silk produced in mammalian cells" *Science* **295**, 472-476

Madsen B. and Vollrath F. (2000) "Mechanics and morphology of silk drawn from anesthetized spiders" *Naturwissenschaften* **87**, 148-153

Menassa R., Zhu H., Karatzas C.N., Lazaris A., Richman A. and Brandle J. (2004) "Spider dragline silk proteins in transgenic tobacco leaves: accumulation and field production" *Plant Biotechnology Journal* **2**, 431-438

Müller U., Jošcák T. and Teischinger A. (2003) "Strength of dried and re-moistened spruce wood compared with native wood" *Holz als Roh- und Werkstoff* **61**, 439-443

Niemz P. (1993) *Physik des Holzes und der Holzwerkstoffe* DRW-Verlag Weinbrenner GmbH & Co, Leinfelden-Echterdingen, Germany p.150

Pérez-Rigueiro J., Elices M., Llorca J. and Viney C. (2001) "Tensile properties of *Argiope trifasciata* drag line silk obtained from the spider's web" *Journal of Applied Polymer Science* **82**, 2245-2251

Pitteroff R. and Woodhouse J. (1998) "Mechanics of the contact area between a violin bow and a string. Part I: Reflection and transmission behaviour" *Acustica* **84**, 543-562

Schuppert J., Private Communication (2005), Max-Planck-Institut für Metallforschung Stuttgart, Abteilung Arzt, Germany

Shao Z. and Vollrath F. (1999) "The effect of solvents on the contraction and mechanical properties of spider silk" *Polymer* **40**, 1799-1806

Spolenak R., Gorb S. and Arzt E. (2005) "Adhesion design maps for bio-inspired attachment systems" *Acta Biomaterialia* **1**, 5-13

Spolenak R., Gorb S., Gao H. and Arzt E. (2005) "Effects of contact shape on the scaling of biological attachments" *Proceedings of the Royal Society London* **A 461**, 305-319

Vincent J.F.V. and Wegst U.G.K. (2004) "Design and mechanical properties of insect cuticle" *Arthropod Structure and Development* **33**, 187-199

Vollrath F. (2000) "Strength and structure of spiders´ silks" *Reviews in Molecular Biotechnology* **74**, 67-83

Wegst, U.G.K. (2004) Natural Materials Selector, created using the CES Constructor Software, Granta Design Ltd. Rustat House, 62 Clifton Road, Cambridge CB1 7EG, UK